Science of the Total Environment 723 (2020) 137896

Contents lists available at ScienceDirect

Science of the Total Environment

journal homepage: www.elsevier.com/locate/scitotenv

Spatiotemporal and probability variations of surface $PM_{2.5}$ over China between 2013 and 2019 and the associated changes in health risks: An integrative observation and model analysis

Zhongjing Jiang [a], Matthew D. Jolleys [b], Tzung-May Fu [c,d,*], Paul I. Palmer [b,*], Yaping Ma [a], Heng Tian [a], Jing Li [a], Xin Yang [c,d]

[a] Department of Atmospheric and Oceanic Sciences, School of Physics, Peking University, Beijing, China
[b] School of GeoSciences, University of Edinburgh, Edinburgh, UK
[c] School of Environmental Science and Engineering, Southern University of Science and Technology, Shenzhen, Guangdong Province, China
[d] Shenzhen Institute of Sustainable Development, Southern University of Science and Technology, Shenzhen, Guangdong Province, China

HIGHLIGHTS

- Annual and seasonal $PM_{2.5}$ concentrations in Chinese cities have decreased since 2013
- Day-to-day variability of $PM_{2.5}$ concentrations is driven by meteorology and chemistry
- Gamma distributions succinctly describe the mean, spread, and skewness of the $PM_{2.5}$ probability distribution
- Health risks due to long-term and short-term exposures to $PM_{2.5}$ have declined in China

GRAPHICAL ABSTRACT

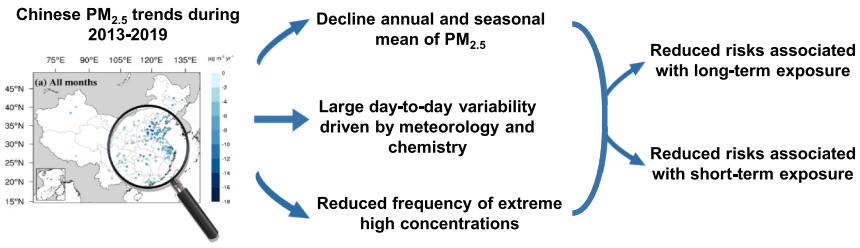

ARTICLE INFO

Article history:
Received 22 October 2019
Received in revised form 10 March 2020
Accepted 11 March 2020
Available online xxxx

Editor: Jianmin Chen

Keywords:
$PM_{2.5}$
Spatiotemporal variability
Probability distribution
Public health
GEOS-Chem model

ABSTRACT

We used statistical methods and the GEOS-Chem model to interpret the observed spatiotemporal and probability variations of surface $PM_{2.5}$ concentrations in China from December 2013 to November 2019, as well as to assess the drivers for the variations and the implications for health risks associated with long-term and short-term exposure to $PM_{2.5}$. Annual and seasonal $PM_{2.5}$ concentrations have decreased over most areas in China during the 6-year period. We decomposed the observed day-to-day variation of $PM_{2.5}$ concentrations in eastern Chinese cities and found that it showed two distinct major spatial modes, which fluctuated in strength seasonally. The first mode, characterized by most of Eastern China being in the same phase, was mainly associated with the regional ventilation of pollutants. The second mode showed a dipolar pattern between the Beijing-Tianjin-Hebei area and the Yangtze River Delta area and was more prominent in summer. Using model simulations, we showed that this dipole mode was chemically driven by the secondary formation of sulfate in summer. We further used a gamma distribution to succinctly interpret the changes in the probability distributions of $PM_{2.5}$. We found that the nationwide decline in seasonal mean $PM_{2.5}$ concentrations mainly reflected decreased occurrences of extremely high $PM_{2.5}$ concentrations, which was strongly driven by the interannual variation of meteorology. These changes in the annual means and probability distributions of $PM_{2.5}$ since December 2013 has led to significant decline of the estimated mortality risks associated with long-term and short-term $PM_{2.5}$-exposures. Regions that were less polluted saw the largest relative benefit per unit decrease in $PM_{2.5}$ concentration, due to the steepness of the exposure-response curve at the low-concentration end. Our integrated methodology effectively diagnosed the

* Corresponding authors.
E-mail addresses: fuzm@sustech.edu.cn (T.-M. Fu), paul.palmer@ed.ac.uk (P.I. Palmer).

https://doi.org/10.1016/j.scitotenv.2020.137896

drivers of $PM_{2.5}$ variability and the associated health risks and can be used as part of the decision tool for $PM_{2.5}$ pollution management over China.

1. Introduction

Particulate matter with an aerodynamic diameter smaller than 2.5 μm ($PM_{2.5}$) has been a frequent culprit of poor air quality in many parts of China (Ministry of Environmental Protection of the People's Republic of China, 2014, 2015, 2016, 2017; Ministry of Ecology and Environment of the People's Republic of China (MEE), 2018, Ministry of Ecology and Environment of the People's Republic of China, 2019), posing great risks to the Chinese public health. In 2013, 99.6% of the Chinese population lived in areas where the annual mean $PM_{2.5}$ concentration exceeded 10 μg m^{-3}, the air quality guideline (AQG) recommended by the World Health Organization (WHO) (Brauer et al., 2016; WHO, 2006). Long-term exposure to annual mean $PM_{2.5}$ concentrations exceeding the AQG is associated with cause-specific mortality (WHO, 2006; Burnett et al., 2014; Song et al., 2017). At the same time, the day-to-day variation of $PM_{2.5}$ concentrations led to excursions of various $PM_{2.5}$ levels, the short-term exposure to which is also associated with significant health risks (e.g., Shang et al., 2013; Lee et al., 2015; Chen et al., 2017b; Liu et al., 2019). In September 2013, the Chinese government promulgated the "Air Pollution Prevention and Control Action Plan" to reduce the anthropogenic emissions of $PM_{2.5}$ and its precursors nationwide (The State Council of the People's Republic of China, 2013). Since then, the annual mean concentrations of $PM_{2.5}$ in many parts of China has decreased (Ministry of Environmental Protection of the People's Republic of China, 2014, 2015, 2016, 2017; MEE, 2018, Ministry of Ecology and Environment of the People's Republic of China, 2019), likely due to both the nationwide emission reduction and the interannual variability of climate (e.g., Zheng et al., 2018; Mao et al., 2019). It is thus crucial to have an updated and comprehensive understanding of the spatiotemporal and probability variations of $PM_{2.5}$, their drivers, as well as the public health implications to better inform policy-making for air quality control.

Exposure to high $PM_{2.5}$ concentrations has been linked with a range of human health problems (WHO, 2006). Cohort studies in China and elsewhere in the world showed that long-term exposure to high $PM_{2.5}$ concentrations above a threshold concentration range may increase the risks of mortality caused by cardiovascular diseases (stroke), ischemic heart disease (IHD), chronic obstructive pulmonary disease (COPD), lung cancer (LC), among other diseases (e.g., Pope et al., 2002; Cao et al., 2011; Fang et al., 2016; Song et al., 2017). Song et al. (2017) estimated that in 2015, long-term exposure to $PM_{2.5}$ may have contributed to 30.2% of the total cause-specific deaths from IHD, stroke, COPD, and LC. On the other hand, short-term exposure to $PM_{2.5}$ have been linked to mortality caused by cardiovascular diseases, hypertension, stroke, respiratory diseases, and COPD, among other diseases (Chen et al., 2017b, Chen et al., 2018; Li et al., 2015; Liu et al., 2019). Chen et al., 2017b estimated a 0.22% increase in daily mortality from total non-accidental causes associated with every 10 μg m^{-3} increase in the two-day running-mean $PM_{2.5}$ concentration. In addition, there is no apparent threshold for the adverse response of human health to short-term exposure of $PM_{2.5}$ (WHO, 2006; Chen et al., 2017b; Liu et al., 2019). Many previous studies have examined the health outcomes of long-term exposure to $PM_{2.5}$ pollution in China and how those health risks may be reduced when annual mean $PM_{2.5}$ levels are reduced (e.g., Cao et al., 2011; Fang et al., 2016; Song et al., 2017; Shi et al., 2018; Ding et al., 2019). Much less is known about the Chinese mortality associated with short-term $PM_{2.5}$ exposure and how those risks are related to the temporal variability of $PM_{2.5}$ concentrations. There is also evidence that different chemical compositions in $PM_{2.5}$ have different toxicity (e.g., Cao et al., 2012; Son et al., 2012), although there is yet insufficient epidemiologic data to formulate the exposure-response relation for individual chemical compositions in $PM_{2.5}$ or for $PM_{2.5}$ from different sources (Burnett et al., 2014).

Temporal and spatial variations of surface $PM_{2.5}$ reflect changes in emissions, atmospheric chemistry, and transport, all of which vary with location and time. For example, $PM_{2.5}$ concentrations over most Chinese cities are higher in winter than in summer (Zhang and Cao, 2015). The higher wintertime $PM_{2.5}$ concentrations are due to a combination of larger anthropogenic emissions from power generation and residential heating (Huang et al., 2017; Ma et al., 2017), a more compressed and stable atmospheric boundary layer that prevents the ventilation of $PM_{2.5}$ to the free troposphere (Guo et al., 2016; Zhong et al., 2018), and reduced wet scavenging by less rainfall (Zhao et al., 2009; Sui et al., 2013). $PM_{2.5}$ concentrations also often show synoptic timescale variation, reflecting the removal of $PM_{2.5}$ by ventilation to the free troposphere and by wet scavenging, both of which processes are associated with the passage of frontal systems (Quan et al., 2014; Shu et al., 2017; Liu et al., 2018; Leung et al., 2018). Many previous studies have examined the national-level patterns and regional-level trends of $PM_{2.5}$ in recent years (e.g., Zhang and Cao, 2015; Silver et al., 2018; Hou et al., 2019; Zhai et al., 2019; Zhang et al., 2019). However, the day-to-day variability of $PM_{2.5}$ and the drivers for that variability, most relevant to the short-term exposure health risks, have not been thoroughly diagnosed.

In this paper, we combined statistical methods and the GEOS-Chem model to present an updated understanding of the spatiotemporal and probability variations of $PM_{2.5}$ concentrations for different parts of China between December 2013 and November 2019. In particular, we emphasized the day-to-day variability of $PM_{2.5}$, its chemical drivers in different seasons, and the changes of that variability since 2013. The identification of the chemical drivers of $PM_{2.5}$ concentration variability may help policy maker to better define emission reduction targets to reduce high $PM_{2.5}$ exposure, as well as better control species-dependent health risks. We introduced the use of the gamma distribution as a succinct way to represent the probability distribution of $PM_{2.5}$ and its changes. We also examined the implications of these observed changes to the $PM_{2.5}$-related health risks associated with both long-term and short-term exposures, with the goal of better informing the next stage of policy-making for air quality management and public health protection.

2. Data and methods

2.1. Chinese network of hourly surface $PM_{2.5}$ measurements

Hourly $PM_{2.5}$ concentrations have been measured since 2013 at a national network of surface sites, managed by the China National Environmental Monitoring Centre (www.cnemc.cn). The number of sites has more than doubled during our study period, from 620 sites in December 2013 to 1640 sites in November 2019, covering 367 cities across China. At each site, $PM_{2.5}$ mass concentrations were measured using either the beta-radiation attenuation method (BAM) or the tapered-element oscillating microbalance method (TEOM) (MEP, 2012; MEP, 2013a). Each site was designed to represent an area in its vicinity of 500 m to 4 km in diameter (MEP, 2013b). The number of sites in each city ranged between 1 and 20, with an average of 4.

These surface $PM_{2.5}$ measurements have not undergone consistent quality assurance/quality control prior to their release to the public and occasionally contained suspect values that may be erroneous. To address this issue, we developed an ad hoc quality control protocol to

remove outliers and invalid measurements (supplementary information). Our protocol was developed independent of those published in a few recent studies but served similar purposes (Barrero et al., 2015; He et al., 2017; Song et al., 2017; Silver et al., 2018). Briefly, we developed five criteria to screen for outliers, continuous repeat values (indicating possible errors in detection or data logging), unrealistic changes, and periods with too few valid measurements. For any given month, sites with <50% valid hourly measurements after applying the quality control were removed from further analysis. Our data quality control removed approximately 2% of the raw hourly data, leaving just over 64 million hourly measurements from all sites for the period between December 2013 and November 2019. For each individual site, 65% to 100% (average 98% for all sites) of the hourly measurements were retained. We then averaged the valid hourly measurement of all available sites within each city to represent the hourly $PM_{2.5}$ level at the city scale. This was done to reduce the sampling bias among cities and to enable comparison with model simulations. Furthermore, data from a city will be removed from all analyses if the valid hourly data was available <85% length of time for each season between December 2013 and November 2019.

2.2. GEOS-Chem model description

We used the GEOS-Chem global 3-D model of atmospheric chemistry and transport (Bey et al., 2001; v11–01, www.geos-chem.org) to simulate surface $PM_{2.5}$ over China from January 2014 to December 2015, in order to help interpret the drivers of the observed $PM_{2.5}$ variability. GEOS-Chem was driven by the GEOS-FP reanalysis meteorological fields from the NASA Global Modeling and Assimilation Office at a native resolution of 0.3125° longitude × 0.25° latitude. Meteorological fields were described on 47 vertical levels extending from the surface to 0.01 hPa, with seven levels below 1 km. The 3-D meteorological data was updated hourly; 2-D data and surface data were updated every 3 h. Boundary layer mixing was described by a non-local scheme to account for differential mixing in response to changing atmospheric instability (Lin and McElroy, 2010).

We used the nested domain capability of GEOS-Chem over Eastern China, defined here as 100–125° E and 20–45° N. This simulation domain, which was a reduced version of the standard GEOS-Chem nested domain for China (Zhang et al., 2016), improved our computation expediency but excluded Heilongjiang, Xinjiang, and Tibet, where there were few $PM_{2.5}$ measurements. Daily lateral boundary conditions were from a self-consistent global GEOS-Chem simulation.

GEOS-Chem included a detailed O_x-NO_x-hydrocarbon-aerosol-bromine chemical mechanism (Parrella et al., 2012; Mao et al., 2013). $PM_{2.5}$ in GEOS-Chem consisted of natural mineral dust, sea salt, primary black carbon aerosols, primary organic aerosols (POA), secondary inorganic aerosols (sulfate, nitrate, and ammonium), and secondary organic aerosols (SOA). Anthropogenic dust was not included in our model version. Natural dust and sea salt aerosols were each represented with four size bins (Fairlie et al., 2007; Jaeglé et al., 2011). Thermodynamics of secondary inorganic aerosols were simulated by the ISORROPIA II package (Fountoukis and Nenes, 2007; Pye et al., 2009). Simulation of primary and secondary organic aerosol was based on the Volatility Basis Set (VBS) (Robinson et al., 2007) as implemented by Pye et al. (2010). POA was treated as semi-volatile or of intermediate volatility (S/IV) and partitioned between the gas and particulate phases (Pye and Seinfeld, 2010). Biogenic SOA was produced by the S/IV oxidation products of isoprene, monoterpenes, and sesquiterpenes. Anthropogenic SOA was produced from the S/IV oxidation products of benzene, toluene, and xylene, as well as from the aging and partitioning of S/IV POA. The organic aerosol to organic carbon mass ratios of 1.4 and 2.1 were assumed for POA and SOA, respectively (Turpin and Lim, 2001).

Chinese monthly anthropogenic emissions of $PM_{2.5}$ primary components and gaseous precursors for the years 2014 and 2015 were from the Multi-resolution Emission Inventory for China (MEIC, v1.3, http://www.meicmodel.org/; Li et al., 2014, Li et al., 2017; Zheng et al., 2018), which included emissions from power generation, industry, transportation, agriculture and residential activities. The native resolution of the inventory was 0.5° longitude × 0.5° latitude which we interpolated to our simulated resolution. Anthropogenic emissions of POA were assigned to two volatility bins (POG1/2) with a ratio of 0.49:0.51. Biogenic volatile organic compound emissions (including isoprene, monoterpenes, and sesquiterpenes) were calculated online using the Model of Emissions of Gases and Aerosols from Nature (MEGAN v2.1, Guenther et al., 2012). Biomass burning emissions were taken from the Global Fire Emissions Database (GFED v4.1s, van der Werf et al., 2010). Emission factors were included for benzene, toluene, and xylene, with emissions of POG1/2 scaled from an OC emission factor and intermediate volatility precursors (IVOCs, distributed as naphthalene) scaled from benzene. Emissions of natural dust and sea salt were as described by Zender et al. (2003) and Jaeglé et al. (2011), respectively.

In order to differentiate the impacts on $PM_{2.5}$ concentrations due to anthropogenic emission reductions and interannual climate variability, we conducted two sets of simulations. The control simulation was driven by year-specific Chinese anthropogenic emissions for 2014 and 2015, respectively. The sensitivity simulation was driven by 2014 Chinese anthropogenic emission only. For comparison against city-scale observations, model results were sampled in each valid observed city at the coordinates of the mass center of the valid sites within that city.

2.3. Decomposition of $PM_{2.5}$ day-to-day variability

We decomposed the observed $PM_{2.5}$ concentrations to examine the spatial patterns associated with the day-to-day variability of $PM_{2.5}$ for each season between December 2013 and November 2019. We also performed the same decomposition to GEOS-Chem simulated results for 2014 to help interpret the observed variability. For the observations in a given season of a given year, we first excluded cities with <90% valid hourly measurements after the quality control. For the remaining cities, we imputed the small number of missing values using mean concentrations of the neighbouring 24 h (more details in the supplementary information). We used a wavelet transform (Torrence and Compo, 1998) as a low-pass filter to remove observed and simulated $PM_{2.5}$ variations at frequencies of less than a day at each city.

We then used empirical orthogonal function (EOF) decomposition (Lorenz, 1956) to reduce the dimensionality of the observed and simulated data to their major spatial modes of variability (i.e., the EOF modes) and the associated timeseries of amplitudes (i.e., the principal components, PCs). The convolution of each EOF mode with its corresponding PC describes the variation of $PM_{2.5}$ attributable to that mode. We divided each year into four seasons: winter (DJF), spring (MAM), summer (JJA), and fall (SON); except that only January and February was used to represent winter 2014 for observation-model comparisons due to the lack of model simulation in December 2013. For each city, the seasonal mean $PM_{2.5}$ concentration for that year was removed prior to the EOF analysis. We assumed that the $PM_{2.5}$ concentrations measured in each city were mutually independent and that measurements at each city carried the same weight. The cities included in the decomposition were consistent throughout the study period for each season, such that the decomposed spatiotemporal modes can be compared between years.

2.4. Gamma distribution fitting of temporal $PM_{2.5}$ probability distribution

We used a two-parameter gamma distribution (Stacy, 1962) to describe the probability density functions (PDFs) of the hourly surface $PM_{2.5}$ concentrations in each city over seasonal time frames (DJF for winter, MAM for spring, JJA for summer, and SON for fall) from December 2013 to November 2019. We also performed the analysis on GEOS-Chem results for January 2014 to November 2015. Several studies have

used the two-parameter gamma distribution to effectively describe the PDF of local particular matter concentrations (e.g., Marani et al., 1986; Rumberg et al., 2001; Sharma et al., 2013). To the best of our knowledge, it has not been applied on a nationwide scale.

We used the maximum likelihood estimation (MLE) method to fit the PDFs of hourly $PM_{2.5}$ concentrations (x) to a two-parameter gamma distribution function $f(x)$ (Eq. (1)):

$$f(x) = \frac{(x/\beta)^{\alpha-1}\ exp(-x/\beta)}{\beta\Gamma(\alpha)} \text{for } x, \alpha, \beta > 0 \quad (1)$$

where α and β are referred to as the shape parameter and the scale parameter, respectively. $\Gamma(\alpha)$ is a gamma function:

$$\Gamma(\alpha) = \int_0^\infty e^{-t} t^{\alpha-1} dt \quad (2)$$

where t is a dummy variable for integration. The mean ($\bar{x}$) and variance (s^2) of the hourly $PM_{2.5}$ concentrations described by the continuous PDF in Eq. (1) can be represented by the products $\alpha\beta$ and $\alpha\beta^2$ (Eqs. (3) and (4)), respectively (Husak et al., 2007):

$$\bar{x} = \alpha\beta \quad (3)$$

$$s^2 = \alpha\beta^2 \quad (4)$$

From Eqs. (3) and (4), β is equivalent to the ratio of the variance and the mean of the continuous PDF ($\frac{s^2}{\bar{x}}$) and therefore represents a measure of the PDF spread. For a given α value, a larger β value indicates a larger spread relative to the mean and a higher probability of very high $PM_{2.5}$ concentrations (Figs. S1a-c). In addition, the gamma distribution is positively skewed; its skewness is equal to $2/\sqrt{\alpha}$, while the excess kurtosis is equal to $6/\alpha$. For a given β value, a smaller α value indicate a more positively-skewed distribution and a relatively higher probability of very low $PM_{2.5}$ concentrations (Figs. S1d-f). As such, the use of the gamma distribution greatly reduces the parameter space required to describe the PDFs of $PM_{2.5}$ concentrations, as well as their changes. The gamma distribution is also a good tool to examine the model's ability to capture the variability when the mean value is well represented. We calculated the values of α and β both at the provincial level, as well as for six regions in China for the purpose of concise presentation: the Beijing-Tianjin-Hebei area (BTH), Northern China (including the BTH area), Northeastern China, Central China, Southern China, and Western China (region divisions are shown in Table S4).

2.5. Health risks associated with long-term and short-term exposure

We assessed the changes in the health risks associated with long-term and short-term exposure of $PM_{2.5}$, as a result of the spatiotemporal changes in $PM_{2.5}$ from December 2013 to November 2019. We calculated the health risks at a provincial level; but for the purpose of concise presentation in Section 5, the results were aggregated to six regions in China.

For long-term exposure, we used the integrated exposure-response (IER) model (Burnett et al., 2014) to calculate the relative risks ($RR_{i,j}$) on a yearly basis for cause-specific mortality for disease j within province i as:

$$RR_{i,j}(C_i) = 1 + a_j\left\{1 - exp\left[-\gamma_j(C_i - C_{0,j})^{\delta_j}\right]\right\}, \text{for } C_i \geq C_{0,j}$$

$$RR_{i,j}(C_i) = 1, \text{for } C_i < C_{0,j} \quad (5b)$$

where C_i was the annual mean $PM_{2.5}$ concentration (μg m^{-3}) for province i. $C_{0,j}$ was the counterfactual (threshold) annual mean $PM_{2.5}$ concentration for disease j, below which there is assumed to be no additional risk for the disease of concern. The parameters, a_j, γ_j, and δ_j, were taken from Song et al. (2017), based on nationally-pooled Chinese mortality data for four specific causes: cerebrovascular disease (stroke), ischemic heart disease (IHD), chronic obstructive pulmonary disease (COPD), lung cancer (LC).

We then calculated the attributable mortality rates (AMR_i) to estimate the total number of cause-specific deaths associated with long-term $PM_{2.5}$ exposure in province i (Song et al., 2017):

$$AF_{i,j} = \frac{RR_{i,j}(C_i) - 1}{RR_{i,j}(C_i)} \quad (6)$$

$$AMR_i = \sum_{j=1}^{n}\left(AF_{i,j} \times y_{i,j}\right) \quad (7)$$

$$AF = \frac{AMR_i}{\sum_{j=1}^{n} y_{i,j}} \quad (8)$$

where $AF_{i,j}$ was the fraction of mortality risk attributable to disease j in province i. $y_{i,j}$ corresponded to the annual standardized mortality rate for disease j in province i, described as deaths per 10^5 people, which were taken from Zhou et al. (2016). AF was the attributable fraction of total deaths caused by $PM_{2.5}$-related stroke, IHD, COPD, and LC. All parameters used in Eqs. (5a), (5b)–(8) are listed in the supplementary information.

For daily mortality associated with short-term exposure of $PM_{2.5}$, we used the Chinese-average $PM_{2.5}$-concentration-response curve derived by Chen et al. (2017b), which described the relative change in daily mortality from all $PM_{2.5}$-related causes as a function of two-day running-mean $PM_{2.5}$ concentrations. Epidemiology studies have found no evidence for a counterfactual concentration (threshold) for health risks associated with short-term $PM_{2.5}$ exposures (e.g., WHO, 2006; Liu et al., 2019). Therefore, we translated the curve such that the relative risk (RR_d) of mortality for zero exposure was zero. Chen et al. (2017b) showed possible decline in RR_d at two-day running-mean $PM_{2.5}$ concentrations >230 μg m^{-3}, although the uncertainty was large. We conservatively assumed RR_d to be constant at two-day running-mean $PM_{2.5}$ concentrations >230 μg m^{-3}. We fitted the resulting exposure-response curve in a piecewise manner (Fig. S2):

$$RR_{d,i}(x_i \leq 50) = 0.0011x_i$$

$$RR_{d,i}(50 < x_i \leq 230) = -4.0433 \times 10^{-7}x_i^2 + 2.3308 \times 10^{-4}x_i + 0.0447$$

$$RR_{d,i}(x_i > 230) = 0.0767 \quad (9c)$$

where x_i (μg m^{-3}) was the two-day running-mean $PM_{2.5}$ concentration in province i, and $RR_{d,i}$ (unitless) was the relative risk of total daily mortality associated with short-term $PM_{2.5}$ exposure in province i. For any given year, we calculated the annual mean relative risk ($RR_{y,i}$) of daily mortality associated with short-term exposure to $PM_{2.5}$ in province i; this was done by weighting the daily relative risk ($RR_{d,i}(x_i)$) with the probability distribution function of x_i in that year and integrating over the full range of x_i.

The exposure-response curves used here for both long-term and short-term exposures were derived from the nationally-pooled mortality data in China (Song et al., 2017; Chen et al., 2017b). Nevertheless, there may be difference in the population's sensitivity to $PM_{2.5}$ in different cities/provinces/regions (e.g., Chen et al., 2017b), either due to spatial inhomogeneity in $PM_{2.5}$ composition, in population physiology, or in medical practices. There are also inevitable representation biases, as $PM_{2.5}$ measurements are sparse in some areas of China (e.g., Western China), where exposure assessment are likely less accurate. We partially, but not entirely, avoid this uncertainty by focusing our analyses

below (Section 5) on the changes within each region for the period between December 2013 and November 2019.

3. Spatiotemporal variation of surface $PM_{2.5}$ in Chinese cities between December 2013 and November 2019 and its drivers

3.1. Spatial patterns and trends of the observed annual and seasonal mean $PM_{2.5}$ concentrations in Chinese cities

Fig. 1 shows the annual and seasonal mean surface $PM_{2.5}$ concentrations from 367 cities in China for the period between December 2013 and November 2019. There was large spatial variability in the annual and seasonal mean surface $PM_{2.5}$ concentrations across China, with the highest concentrations generally found over Northern China (Fig. 1a). Surface $PM_{2.5}$ concentrations in most cities were higher in winter months and lower in summer months, as shown in previous studies (e.g., Zhang and Cao, 2015). Wintertime average $PM_{2.5}$ concentrations exceeded 75 μg m^{-3} over Northern China (Fig. 1b). The concentrations and spatial patterns of $PM_{2.5}$ were similar in spring and fall (Fig. 1c and e), with the exception of a few cities in Xinjiang Province in spring, likely reflecting the impact of natural dust (Xue et al., 2010; Turap et al., 2019). In summer, the mean $PM_{2.5}$ concentrations were below 75 μg m^{-3} in almost all Chinese cities (except the city of Hetian in Xingjiang) and below 35 μg m^{-3} (first interim target recommended by the WHO, IT-1) in 77% of the cities (Fig. 1d).

Fig. 2a shows the observed trends in annual mean $PM_{2.5}$ concentrations at the 189 valid cities (188 for DJF, 187 for MAM, 188 for JJA, 189 for SON) between December 2013 and November 2019. Fig. S3 shows the observed trends in percentages relative to the mean. Out of those 189 cities, 155 showed significant negative trends (p-values < 0.1) in the annual mean $PM_{2.5}$. The remaining 34 cities showed no significant trends during this period in the annual means. Silver et al. (2018) previously analyzed a shorter $PM_{2.5}$ record (January 2015–December 2017) and found significant positive trends in annual mean $PM_{2.5}$ at 10% of the cities, mainly over Shanxi and Jiangxi provinces. We found that those positive trends were driven by brief increases in $PM_{2.5}$ concentrations in 2017 in those two provinces. We found no significant annual trends in those cities

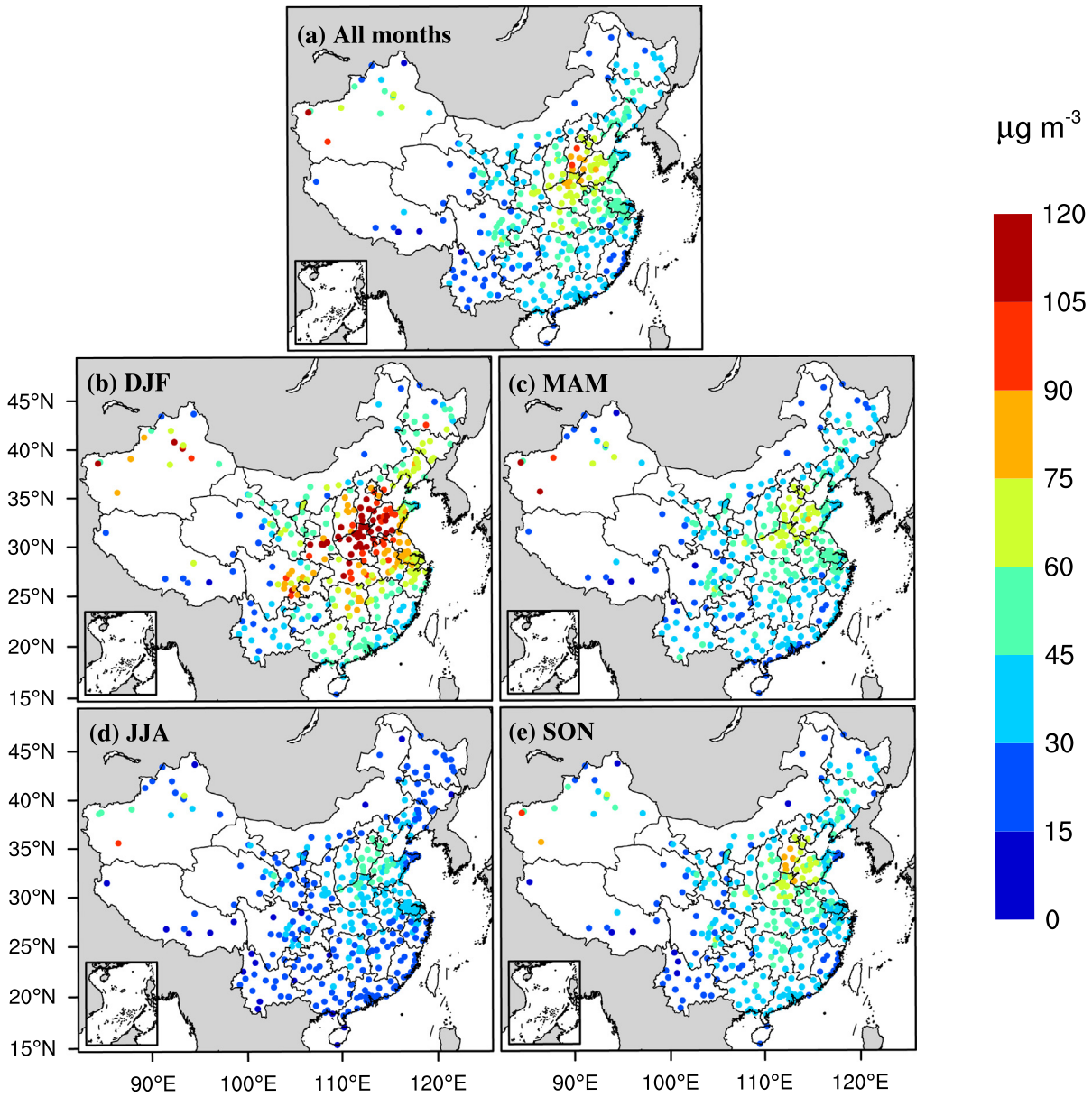

Fig. 1. Observed annual and seasonal mean surface $PM_{2.5}$ concentrations (μg m^{-3}) from the national monitoring network over China during December 2013 to November 2019: (a) all months, (b) winter (DJF), (c) spring (MAM), (d) summer (JJA), and (e) fall (SON).

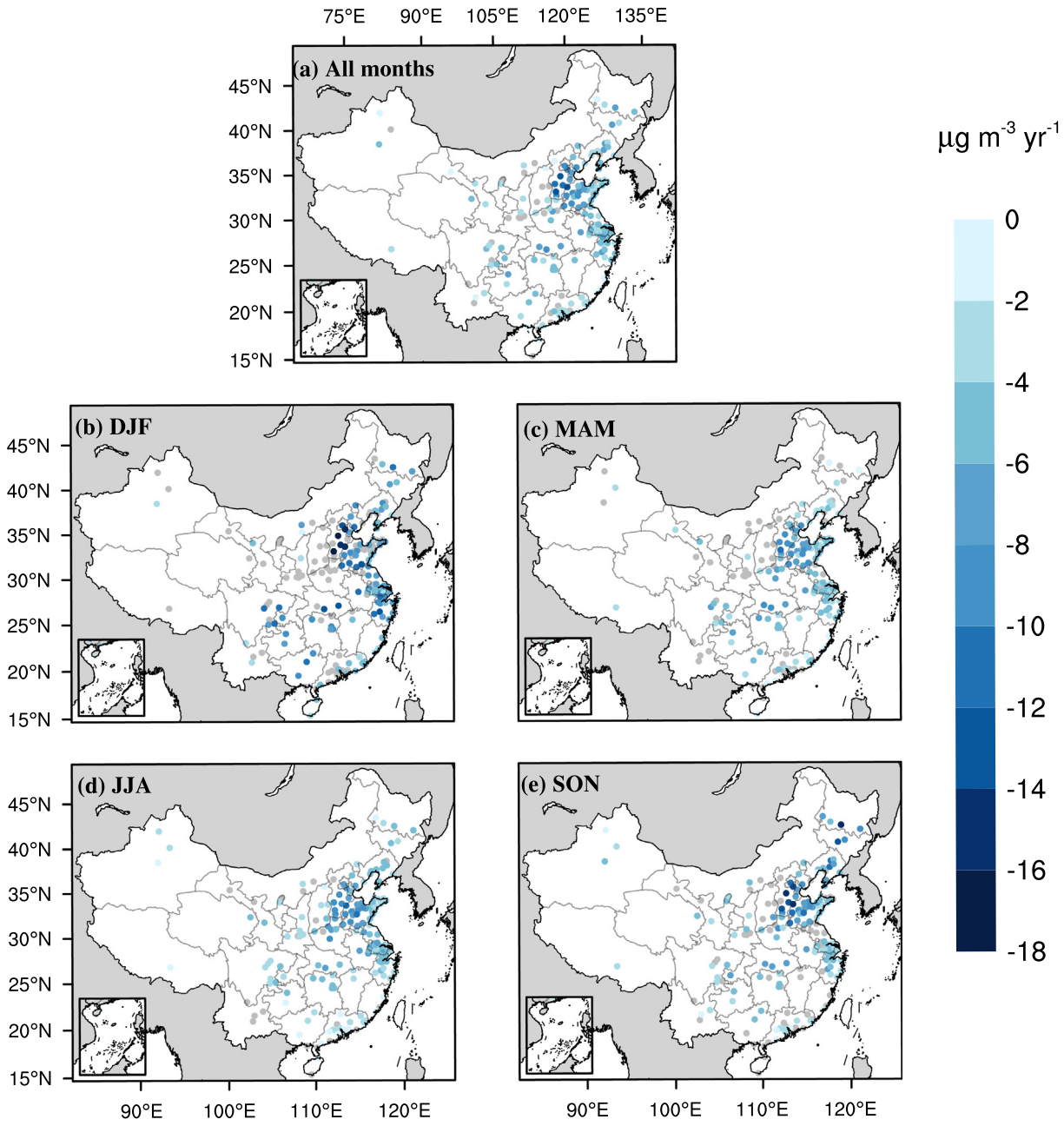

Fig. 2. Trends of $PM_{2.5}$ concentrations (μg m^{-3} yr^{-1}) for (a) all months and for different seasons: (b) winter (DJF), (c) spring (MAM), (d) summer (JJA), and (e) fall (SON) during December 2013 to November 2019. Blue dots represent cities with significant negative trends of $PM_{2.5}$ concentrations (significance level = 0.1). Gray dots represent cities with no significant trends. (For interpretation of the references to colour in this figure legend, the reader is referred to the web version of this article.)

after re-analyzing the $PM_{2.5}$ data using our longer dataset. Figs. 2b-2e show the observed trends of seasonal mean $PM_{2.5}$ concentrations from December 2013 to November 2019. For cities with sufficient valid data, 109 (out of 188 in DJF), 128 (out of 187 in MAM), 163 (out of 188 in JJA), and 127 (out of 189 SON) cities showed significant negative trends in seasonal mean $PM_{2.5}$ concentrations. The rest of the cities showed no significant trends.

Fig. 3 shows the monthly and annual mean $PM_{2.5}$ concentrations from December 2013 to November 2019 for the three largest megacity clusters in China: the Beijing-Tianjin-Hebei area (BTH), the Yangtze River Delta (YRD), and the Pearl River Delta (PRD). Despite the large seasonal and interannual variations, the annual mean $PM_{2.5}$ concentrations for all three megacity clusters showed significant negative linear trends: −8.1, 4.4, and −2.2 μg m^{-3} yr^{-1} for the BTH, the YRD, and the PRD, respectively. The annual mean concentration of $PM_{2.5}$ in the PRD has remained below the WHO IT-1 of 35 μg m^{-3} since 2015. $PM_{2.5}$ concentrations in all three megacity clusters peaked in winter. Wintertime $PM_{2.5}$ concentrations in the BTH area showed larger year-to-year variation compared to the other clusters, which likely indicated a stronger influence of meteorology to wintertime $PM_{2.5}$ for the BTH area (Mao et al., 2019). It is also possible that interannual variation of anthropogenic emissions, for example that related to differences in power consumption, may be partially contributing to the larger interannual variation of wintertime $PM_{2.5}$ concentration in the BTH area. We also note that the secondary $PM_{2.5}$ peak in the BTH area in summer (June and July) has disappeared since 2017. This is likely related to the ban on the open-burning of crop residue in Northern China, which used to be a major source of seasonal pollutantants after the local wheat harvest in early summer (Chen et al., 2017a).

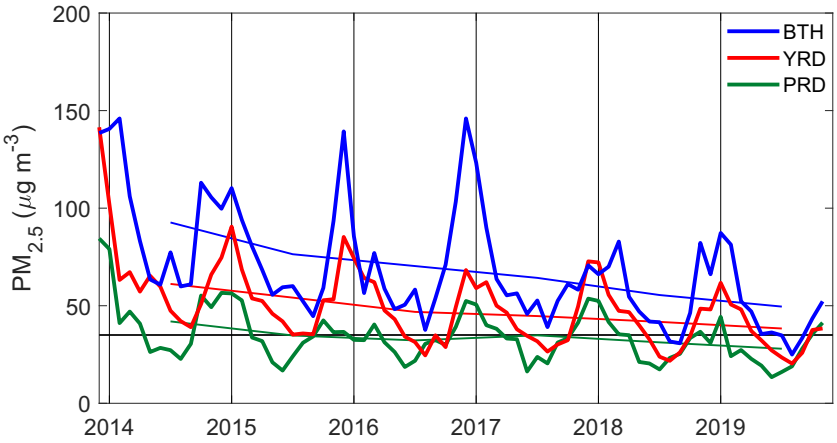

Fig. 3. Time series of the observed monthly (thick) and annual (thin) mean $PM_{2.5}$ concentrations from December 2013 to November 2019 for three major megacity clusters in China; Beijing-Tianjin-Hebei (BTH, blue), Yangtze River Delta (YRD, red), and Pearl River Delta (PRD, green). The vertical black lines indicate January of each year. The horizontal black line indicate the World Health Organization interim target-1 standard (IT-1) of 35 μg m^{-3}. (For interpretation of the references to colour in this figure legend, the reader is referred to the web version of this article.)

3.2. Day-to-day variation of $PM_{2.5}$ concentrations over eastern Chinese cities

We next examined the day-to-day variation of $PM_{2.5}$ concentrations in Eastern China for different seasons. Fig. 4 shows the first two leading EOFs of the day-to-day variation of $PM_{2.5}$ and their explained variance for the four seasons from December 2013 to November 2019. The cities used for the analysis in Fig. 4 are consistent for each season (108 for winter, 174 for spring, 172 for summer, and 176 for fall), such that the observed EOF modes can be compared for the years 2014 to 2019. The day-to-day variation of the observed $PM_{2.5}$ over Eastern China mostly showed two distinct spatial patterns in all seasons during the 6 years. One characteristic EOF mode showed a spatial pattern with most of Eastern China in the same phase and with the largest amplitude over Northern China, including the BTH area and nearby provinces of Shandong and Henan. This pattern likely reflected the regional ventilation of $PM_{2.5}$ over Eastern China associated with the passages of cold fronts, which have the largest impacts on $PM_{2.5}$ concentrations over the highly polluted Northern China area (e.g., Liu et al., 2018). The other EOF mode showed a dipole pattern, where the BTH area and the YRD area were in opposite phases. These findings were consistent with the analysis by Liu et al. (2018), although the spatial extent of their analysis only covered Northern and Central China and was limited to studying fall and winter months in 2013.

We found, however, that the relative importance of these two observed spatial modes of $PM_{2.5}$ variability differed by season. In winter, spring, and fall, the in-phase mode contributed 26% to 48% of the observed synoptic variance of $PM_{2.5}$ in Eastern China, while the dipole mode contributed only 10% to 18% of the observed variance. In contrast, during summer months, the contribution of these two spatial modes to the observed $PM_{2.5}$ variability was similar (15% to 20% for the in-phase mode and 11% to 20% for the dipole mode, respectively). The exception

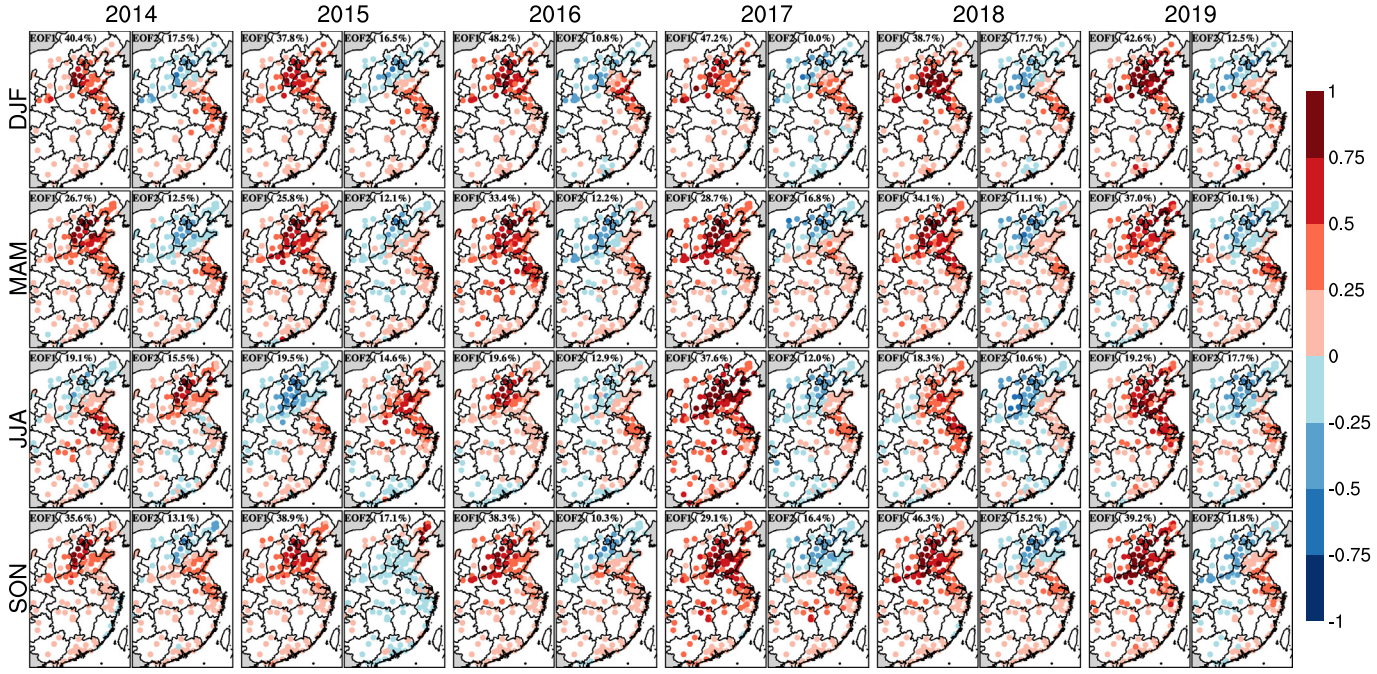

Fig. 4. The first and second EOF modes for the observed day-to-day variation of $PM_{2.5}$ concentrations over Eastern China for winter (DJF), spring (MAM), summer (JJA), and fall (SON) during December 2013 to November 2019. The percentages of variance explained by each mode are in the parentheses.

was summer 2017, when the in-phase mode explained 37.6% of the observed variance. For their analysis of fall and winter only, Liu et al. (2018) attributed both spatial modes to wind-related dilution or build-up of pollutants by virtue of their similarity to EOF spatial patterns found in wind speed for the same period. We found below, however, that chemical drivers may also contribute to the relative strengths of the two spatial modes.

3.3. Chemical drivers of the observed day-to-day variation of $PM_{2.5}$ concentrations over eastern Chinese cities

We used the GEOS-Chem model to interpret the chemical drivers of the observed $PM_{2.5}$ day-to-day variation modes using the year 2014 as an example. To achieve this, we first examined the model's ability in describing the observed seasonal mean concentrations and modes of $PM_{2.5}$ day-to-day variation in 2014. Fig. S4 compares the observed and GEOS-Chem-simulated seasonal mean $PM_{2.5}$ concentrations in 2014 over Eastern Chinese cities. For the purpose of comparing model and observations, only January and February 2014 were used to represent winter 2014, due to a lack of model simulation in December 2013. The GEOS-Chem model was able to reproduce the observed seasonal spatial distributions of $PM_{2.5}$. The spatial correlation coefficients (R) between the observed and simulated seasonal mean $PM_{2.5}$ concentrations for the four seasons were between 0.72 and 0.85. However, the model generally underestimated the observed $PM_{2.5}$ concentration in Chinese cities. The model biases against the observed seasonal mean $PM_{2.5}$ over Eastern China were −21% (winter), −20% (spring), −24% (summer), and −27% (fall), respectively.

Fig. 5 compares the first two leading EOFs in the observed and simulated $PM_{2.5}$ day-to-day variation for the four seasons in 2014. Fig. 6 shows the observed and simulated principal components (PCs) that correspond to these two leading EOFs. We found that the GEOS-Chem model was able to reproduce both spatiotemporal modes of $PM_{2.5}$ day-to-day variability, as well as the seasonal differences in the relative

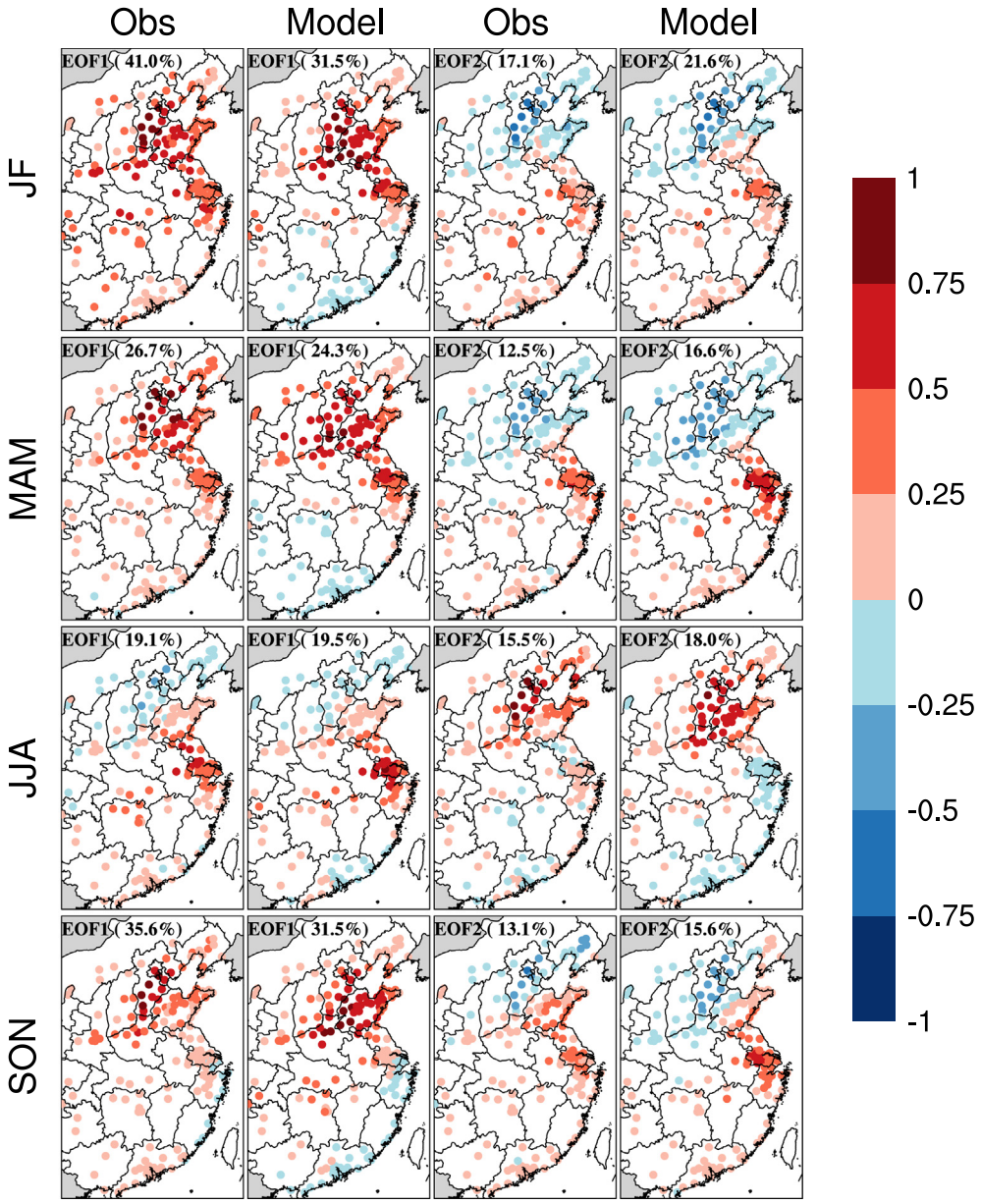

Fig. 5. Comparison of EOFs for the observed and simulated $PM_{2.5}$ concentrations over Eastern China for winter (JF), spring (MAM), summer (JJA), and fall (SON) in 2014. The first and third columns are the first and second EOFs for the observations, respectively. The second and fourth columns are the first and second EOFs for the simulation, respectively. Blue and red colors indicate opposite amplitudes around the seasonal mean $PM_{2.5}$ concentration at each city. The percentages of variance explained by each mode are in the parentheses. (For interpretation of the references to colour in this figure legend, the reader is referred to the web version of this article.)

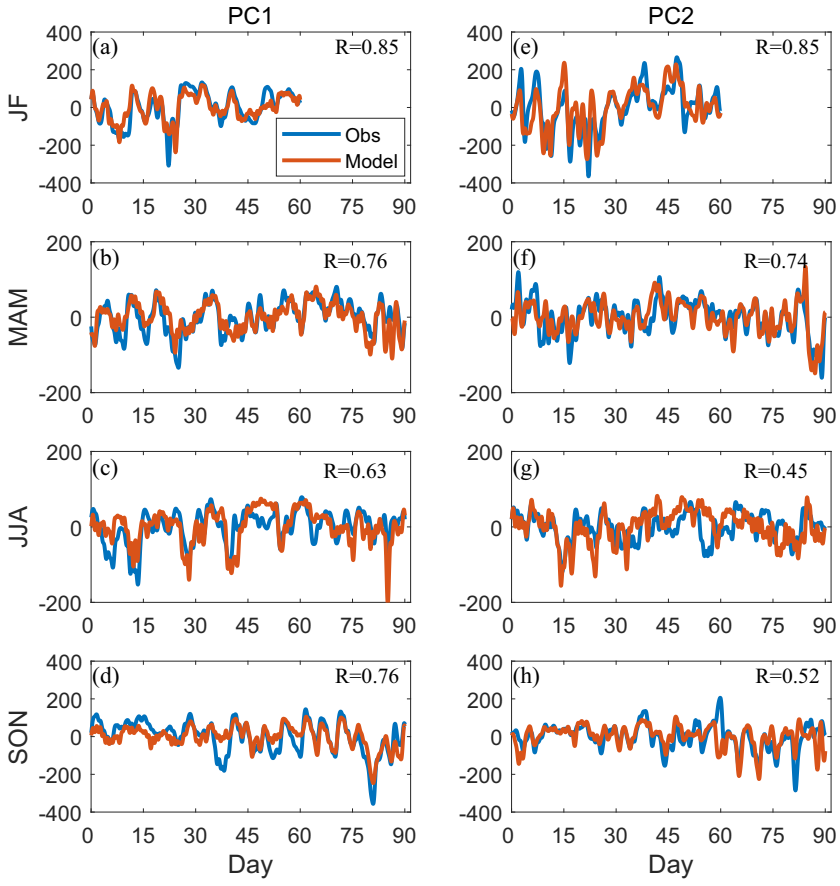

Fig. 6. The principle components (PC) of the first (left panel) and second (right panel) EOF modes for the day-to-day variability of observed (blue) and simulated (red) $PM_{2.5}$ over Eastern China for winter (JF), spring (MAM), summer (JJA), and fall (SON) in 2014. (a and e) JF, (b and f) MAM, (c and g) JJA, (d and h) SON. The correlation coefficients between the observations and the simulated results are shown inset. The y-axis show the temporal variation of the relative amplitudes of the EOF modes shown in Fig. 5. (For interpretation of the references to colour in this figure legend, the reader is referred to the web version of this article.)

contributions of the two modes. The cities used for the analysis in Fig. 5 are consistent for each season (176 for winter (JF), 174 for spring, 172 for summer, and 176 for fall). The spatial correlation coefficients between the observed and simulated EOF modes ranged from 0.70 to 0.91 for different seasons (Fig. 5). The temporal correlation coefficients between the observed and simulated PCs ranged from 0.45 to 0.85 for different seasons (Fig. 6). This provided us with confidence that the GEOS-Chem model could be used to examine the drivers of the observed day-to-day $PM_{2.5}$ variability.

Fig. 7 shows the first EOF modes of the day-to-day variability of $PM_{2.5}$ and its chemical components, as simulated by GEOS-Chem for different seasons in 2014. Fig. S5 shows the mass percentage of individual chemical components in total $PM_{2.5}$ for different seasons. The leading EOF for the primary $PM_{2.5}$ components (BC, natural dust, sea salt) showed seasonal patterns characteristic of their sources and their regional removal by ventilation. For example, the first EOF of BC, which is mostly emitted by anthropogenic sources in China (Yang et al., 2017), showed the in-phase pattern in all seasons. This reflected the large emission of primary anthropogenic pollutants in Northern China, as well as their ventilation by the passage of cold fronts (Liu et al., 2018). Anthropogenic dust was not included in our model version, but its major EOF mode of variability would likely be similar to that of BC, owing to their common combustive source in China (Philip et al., 2017). In contrast, the first EOF of natural dust showed larger amplitudes over Western and Northern China and lower amplitudes over Southern China, particularly in spring, reflecting seasonal dust emissions from the arid Western and Northern China. The variability mode of sea salt was distinctively coastal, particularly in the YRD area in winter and fall and in the PRD in spring.

Fig. 7 also showed the day-to-day variation of secondary aerosols (including sulfate, nitrate, ammonium, anthropogenic SOA, biogenic SOA) simulated by GEOS-Chem model. The first EOFs for nitrate and ammonium reflected the "in-phase" pattern in all seasons in 2014. In contrast, the first EOF of sulfate and anthropogenic SOA both showed the dipole pattern in summer, where the high amplitudes over the YRD and the BTH areas were of opposite signs. The first EOF of biogenic SOA showed largest amplitudes over Central and Southern China, reflecting the stronger SOA sources there (Fu et al., 2012). As simulated by the GEOS-Chem model, sulfate was the second largest chemical component in $PM_{2.5}$ following nitrate throughout Eastern China in summer (Fig. S5). In other words, the major source of $PM_{2.5}$ variability over Eastern China in summer was due to secondary sulfate formation, especially over the YRD area. The variability of BC and ammonium was also slightly enhanced over YRD during summer months due to the seasonal crop residue burning in June and July over the YRD area (Chen et al., 2017a).

Our findings were consistent with some previous studies (Zhang et al., 2011; Zhang et al., 2017). Zhang et al. (2011) analyzed monthly aerosol composition at 16 urban, rural, and remote sites across China and found that the seasonal variation of sulfate were generally consistent with those of carbonaceous aerosols (OC, EC), except for a distinct increase in June and July, particularly at urban sites. In a review paper, Zhang et al. (2017) synthesized individual published datasets, and in the absence of widespread measurements of $PM_{2.5}$ chemical components, concluded that secondary inorganic sources contributed more to total $PM_{2.5}$ in the southern and central China. Our work complemented these studies by using EOFs to examine the variability of the $PM_{2.5}$ components in the model, which reflected their sources, atmospheric transport, and removal processes. Until a speciated

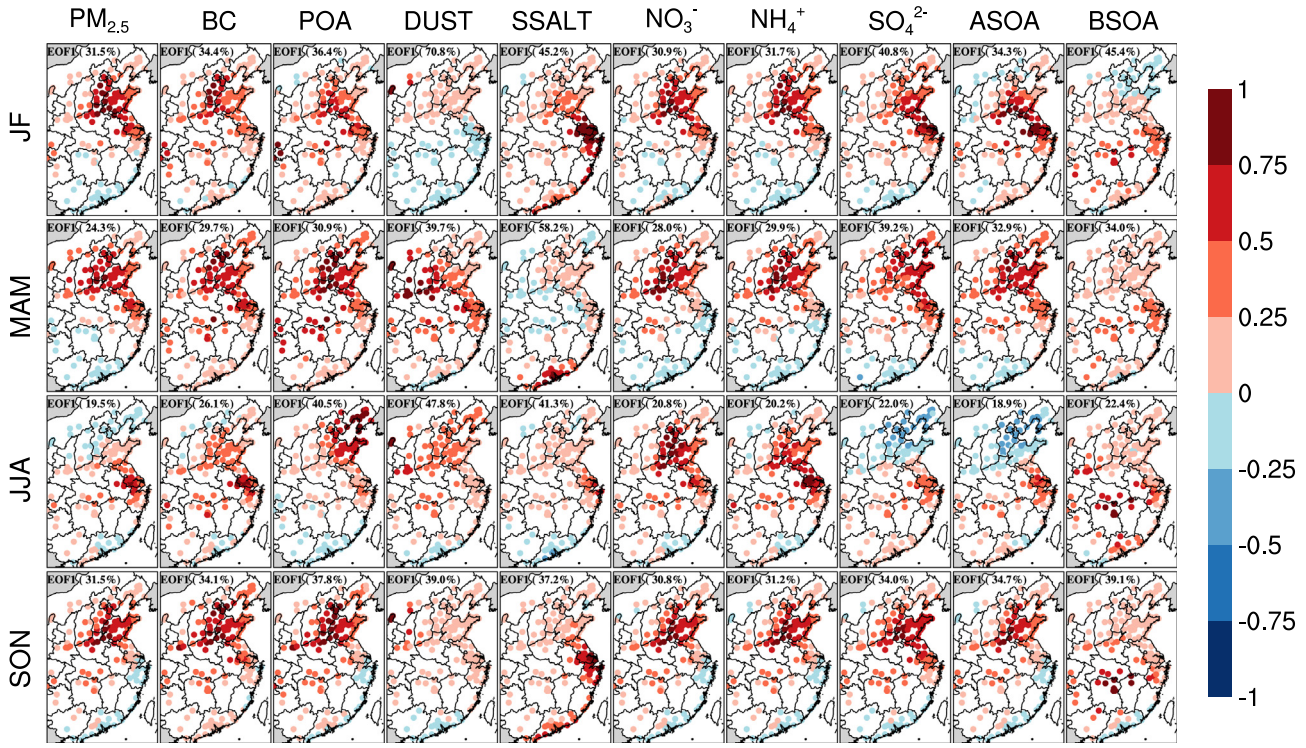

Fig. 7. The first EOF mode of simulated total $PM_{2.5}$, four primary $PM_{2.5}$ components (BC, primary organic aerosol, dust, and sea salt), three secondary inorganic components (NO_3^-, NH_4^+, SO_4^{2-}), and two SOA components (anthropogenic SOA and biogenic SOA). Each column represents a component and four rows represent different seasons in 2014. ASOA is aromatic SOA and BSOA is the sum of isoprene and terpene SOA.

measurement network becomes available across China, we demonstrated here that a model-based analysis could be used to attribute observed variation of total $PM_{2.5}$ to variation in the individual $PM_{2.5}$ components. This helps policy makers to formulate more effective emission reduction strategies to limit exposure and public health risks, especially when species-dependent health risks become better understood.

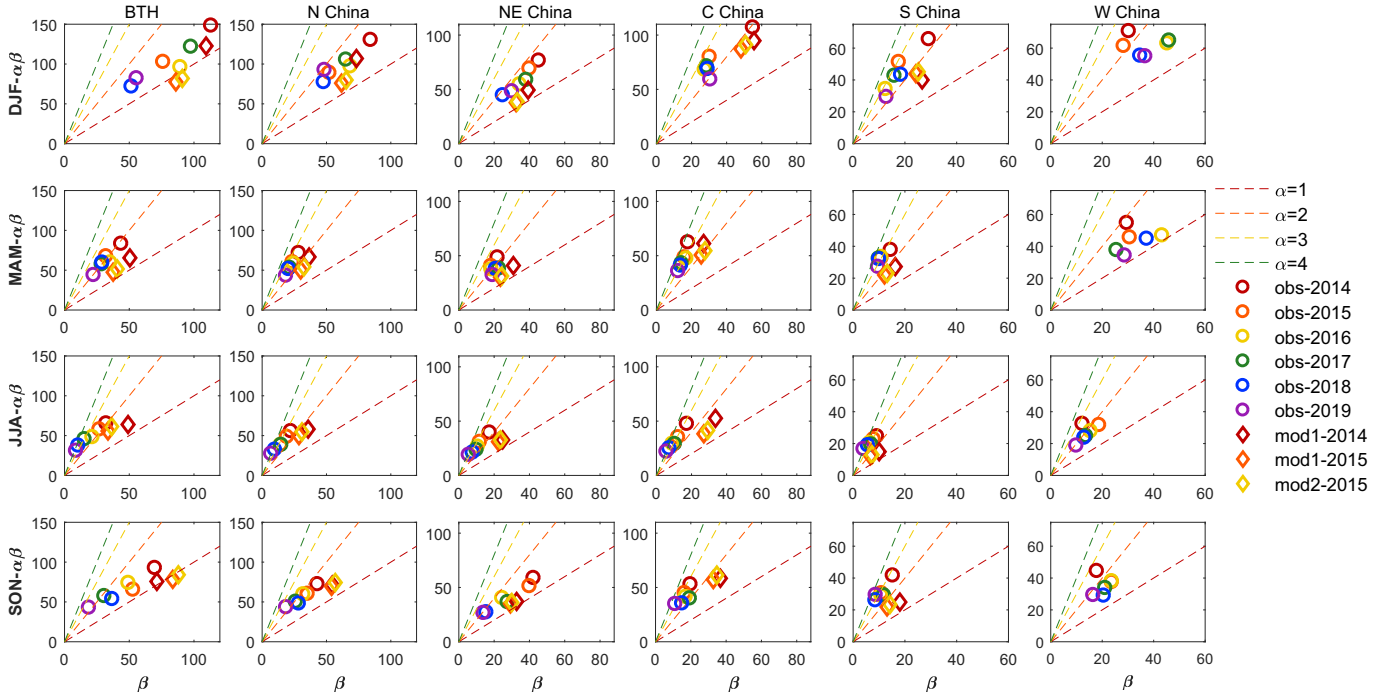

Fig. 8. Changes in the gamma distribution function parameters for the observed and simulated probability distribution of hourly $PM_{2.5}$ in six regions in China for each of the four seasons during December 2013 to November 2019. For each subplot, the values of the β parameter are shown in the horizontal direction, while the seasonal mean $PM_{2.5}$ concentrations (equivalent to αβ) are shown in the vertical direction. The values of the α parameter are shown by the slope (colored dashed lines). Circles markers show observed values for each region for different years (2014, red; 2015, orange; 2016, yellow; 2017, green; 2018, blue; 2019, purple). Diamond markers represent simulated values for each region for 2014 (red) and 2015 (orange). Also shown are the values from a sensitivity simulation for 2015 driven by 2014 anthropogenic emissions (yellow diamond). Western China was not simulated. Note the variable axis scales. (For interpretation of the references to colour in this figure legend, the reader is referred to the web version of this article.)

4. Changes in the probability distributions of observed $PM_{2.5}$ concentrations in Chinese cities between December 2013 and November 2019

Our analyses in Section 3 showed changes in the observed annual and seasonal mean $PM_{2.5}$ concentrations since 2013. Here we demonstrated the use of the parameters (α and β) of the gamma distribution function (Section 2.4) as an effective way to represent and interpret the observed changes in the full PDF of $PM_{2.5}$. Fig. 8 shows the observed seasonal changes of mean $PM_{2.5}$ concentrations ($=\alpha\beta$) and α and β parameters in six Chinese regions between December 2013 and November 2019. Across all regions, there were significant seasonal differences in the mean $PM_{2.5}$ concentrations (Fig. 1) that were associated with seasonal variations in both α and β, although the seasonal variation in β were more prominent. The mean $PM_{2.5}$ concentrations and β values were generally highest in BTH and Northern China, across all years and seasons. This indicated more frequent occurrences of extreme-high $PM_{2.5}$ events in Northern China. Since December 2013, the seasonal mean $PM_{2.5}$ concentrations in most regions have decreased (Fig. 2), particularly in fall and winter. These changes were mainly driven by decreases in β values. In other words, the changes in seasonal mean $PM_{2.5}$ concentrations were predominantly driven by less frequent occurrences of extremely high $PM_{2.5}$ concentrations. The changes in α since December 2013 were less evident across the country, indicating less changes in the frequency of extreme-low $PM_{2.5}$ conditions.

Fig. 8 also shows the seasonal changes in mean $PM_{2.5}$ concentrations and α and β values from our GEOS-Chem sensitivity simulations for the years 2014 and 2015, which elucidate the drivers of the observed changes in $PM_{2.5}$ PDF. As previously discussed in Section 3.3 (Fig. S4), the model was able to reproduce the seasonal mean $PM_{2.5}$ concentration over Eastern China (Western China was not simulated). However, the model slightly overestimated β (and underestimate α) in BTH and Central China in spring, summer, and fall of 2014, while underestimating β in Northeastern China (and overestimating α) in Southern China and in fall and winter of 2014. We found that there were significant decreases in the simulated β values for most regions between 2014 and 2015, consistent with the observations. Using sensitivity simulations driven by constant anthropogenic emissions (locked at 2014 levels), we found that the large observed and simulated changes in β values were mainly driven by the difference in meteorology, and not by the difference in emission, between 2014 and 2015. In comparison, neither the difference in meteorology nor the difference in emission between 2014 and 2015 led to much changes in the α parameters across China.

Our sensitivity simulations for the years 2014 and 2015 only involved relatively small difference in Chinese anthropogenic emissions, but Chinese anthropogenic emissions had continued to decrease after 2015. Zheng et al. (2018) estimated that the Chinese annual anthropogenic SO_2 emission in 2015 was 17% lower than that in 2014, but the annual anthropogenic SO_2 emission in 2017 was 49% less than that in 2014. As such, the dramatically reduced Chinese anthropogenic emissions since 2013 likely played a stronger role in reducing the observed mean $PM_{2.5}$ concentrations and β values across China between 2013 and 2019 than indicated here. Nevertheless, our results emphasized the very large impacts of the interannual variation in meteorology in the observed decline of mean $PM_{2.5}$ concentrations and the decreased frequencies of extremely high $PM_{2.5}$ conditions across China since 2013, consistent with the previous analysis of Mao et al. (2019).

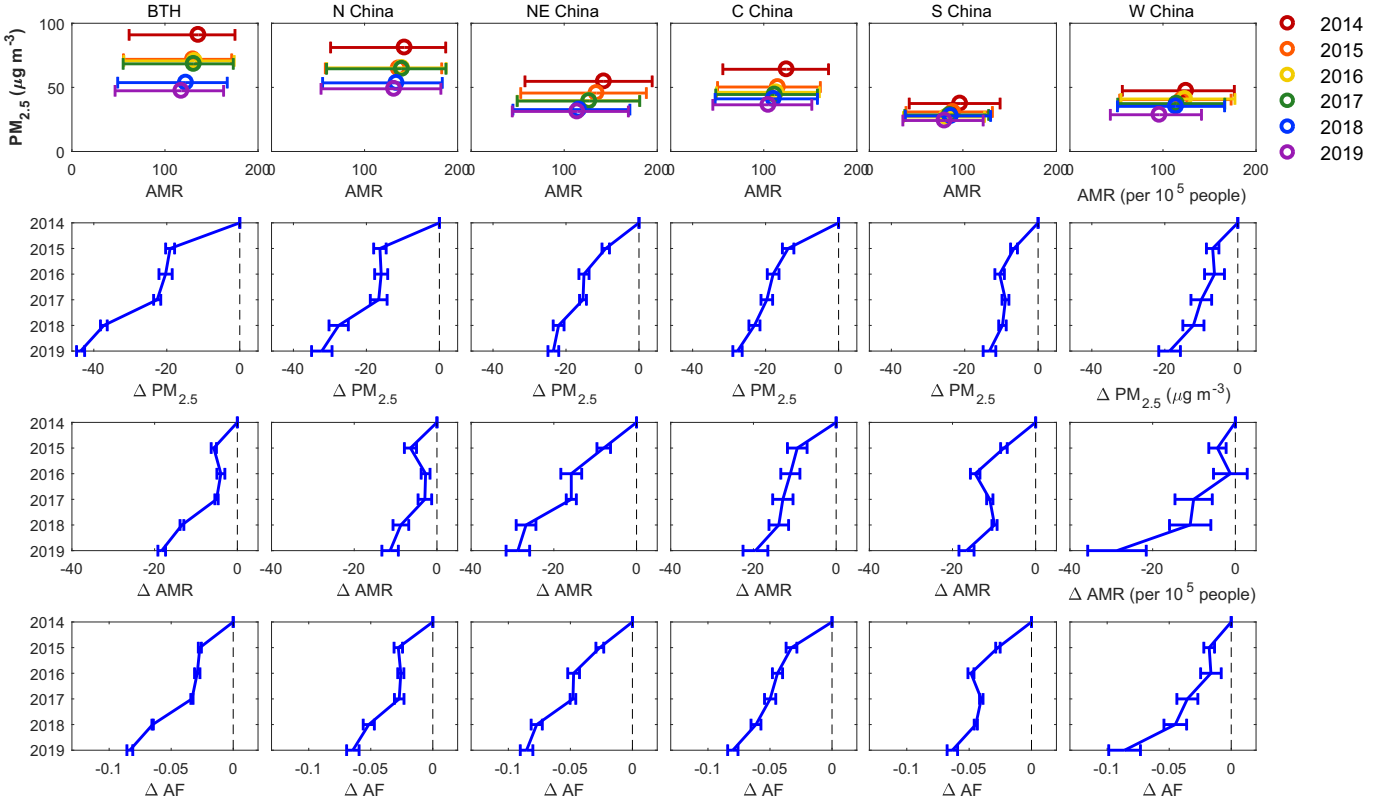

Fig. 9. Annual changes in health risks associated with long-term exposure to $PM_{2.5}$ in six Chinese regions between 2014 and 2019. First row: the regional annual attributable mortality rates (AMR, per 10^5 people) of $PM_{2.5}$-related stroke, IHD, COPD, and LC, as a function of annual regional mean $PM_{2.5}$; the error bars represent the 95% confidential intervals of AMR. The years are colour-coded. Second row: differences in regional annual mean $PM_{2.5}$ concentration relative to 2014 ($\Delta PM_{2.5}$, $\mu g\ m^{-3}$). Third row: differences in regional annual AMR (ΔAMR, per 10^5 people) relative to 2014. Fourth row: differences in regional annual fraction (ΔAF, unitless) of cause-specific mortality attributable to $PM_{2.5}$ long-term exposure relative to 2014. The error bars in the second to fourth row represent the standard deviation in the region for each year.

5. Changes in the health risks associated with long-term and short-term exposures to $PM_{2.5}$ in China during 2014 to 2019

Finally, we examined the health outcomes associated with long-term and short-term exposures to $PM_{2.5}$ in China during winter 2014 (December 2013 to February 2014) to fall 2019 (September to November 2019). Several previous studies have presented epidemiological analyses of $PM_{2.5}$ related health outcomes in China and the changes in recent years. Here we focused on how the changes in $PM_{2.5}$-related health risks were related to the observed changes in the annual means and PDFs of $PM_{2.5}$ since 2014. For the purpose of presentation, each year was represented by the period from December of the previous year to November of the current year.

Fig. 9 shows the estimated annual cause-specific (stroke, IHD, COPD, and LC) AMR (per 10^5 people) associated with long-term $PM_{2.5}$ exposure in six Chinese regions between 2014 and 2019, along with the 95% confidence intervals of the estimated AMR. Although there is considerably large uncertainty to the estimated value of AMR, the mean estimated annual AMR values have decreased since 2014 as a result of the declines in annual mean $PM_{2.5}$ in all regions. The largest AMR changes were in Northeastern and Western China, where the AMRs in 2019 were reduced by 29 deaths per 10^5 people relative to 2014. Because the AMRs are highly sensitive to the age-standardized cause-specific mortality rates in each region, we also examined the fractions of cause-specific mortality attributable to $PM_{2.5}$ long-term exposure (AF), which provided a normalized measure of cause-specific mortality. Fig. 9 shows the changes in regional annual average AF, while Fig. S6 shows the annual average AF for each city between 2014 and 2019. As shown in Fig. 9, the AFs have also decreased in all regions, with largest changes approaching 9% in Northeastern and Western China in 2019 relative to 2014.

An interesting feature to note is that, for a unit decrease in $PM_{2.5}$, the relative decrease in AF was also largest in Western and Southern China. The slopes of the regression lines for ΔAF versus $\Delta PM_{2.5}$ between 2014 and 2019 were 0.0019 (BTH), 0.0020 (Northern China), 0.0036 (Northeastern China), 0.0028 (Central China), 0.0048 (Southern China), and 0.0047 (Western China), respectively. This reflected the fact that the shape of the exposure-response curve for $PM_{2.5}$-related health risks was steeper at low $PM_{2.5}$ concentrations (Eqs. (5a), (5b); Burnett et al., 2014; Song et al., 2017). As such, the reduction of annual mean $PM_{2.5}$ concentrations in less polluted regions would lead to largest relative benefit in AF. Cause-specific and total annual mean AF, AMR at the province level, as well as the lower and upper values of the 95% confidence intervals, are given in Tables S4–S9. Averaged AF values for four diseases at the city-level between 2014 and 2019 are shown in Fig. S6.

We further evaluated the annual mean relative risks (RR_y) of daily mortality associated with short-term $PM_{2.5}$ exposure in six Chinese regions between 2014 and 2019 (Fig. 10). As described in Section 2.5, the daily mortality associated with short-term $PM_{2.5}$ exposure is dependent on the two-day running-mean $PM_{2.5}$ concentrations. As such, it is likely to be sensitive to the changes in the PDF of $PM_{2.5}$. The second row in Fig. 10 shows the RR_y between 2014 and 2019 calculated with the observed PDF of $PM_{2.5}$, as well as the RR_y calculated by applying different assumptions to the PDF. The RR_y calculated with the observed $PM_{2.5}$ concentrations showed significant reduction across all regions since 2014. Again, the changes in RR_y per unit change in annual mean $PM_{2.5}$ were largest in Southern and Western China, reflecting the steepness of the exposure-response curve at low $PM_{2.5}$ concentrations (Eq. (9a), (9b), (9c); (Chen et al., 2017b). We found the PDFs of the $PM_{2.5}$ concentrations were indeed important for short-term exposure. The RR_y calculated using only the annual mean $PM_{2.5}$ concentrations were consistently larger than the real RR_y, also due to the much lower risks at the low-end of $PM_{2.5}$ concentrations.

Also in Fig. 10, we hypothetically calculated the changes in RR_y using the observed year-specific annual mean $PM_{2.5}$ concentrations ($=\alpha\beta$), while locking α and β to their 2014 values, respectively. Theoretically, larger RR_y reduction can be gained by decreasing α values, which indicate more frequent occurrences of extreme-low $PM_{2.5}$. However, because α values have not changed much since 2014 (Fig. 8), the actual decreases in RR_y across China since 2014 were mainly driven by the decline of the β values.

Our analyses in Figs. 9 and 10 show that the health risks associated with both long-term and short-term exposure to $PM_{2.5}$ have both decreased since 2014. Even steeper decline in the health risks can be expected if $PM_{2.5}$ were further reduced, as nation-wide concentrations move toward the steeper part of the exposure-response curves. In addition, if α decreases, the relative decline in RR_y for a given reduction in annual mean $PM_{2.5}$ concentration would be enhanced.

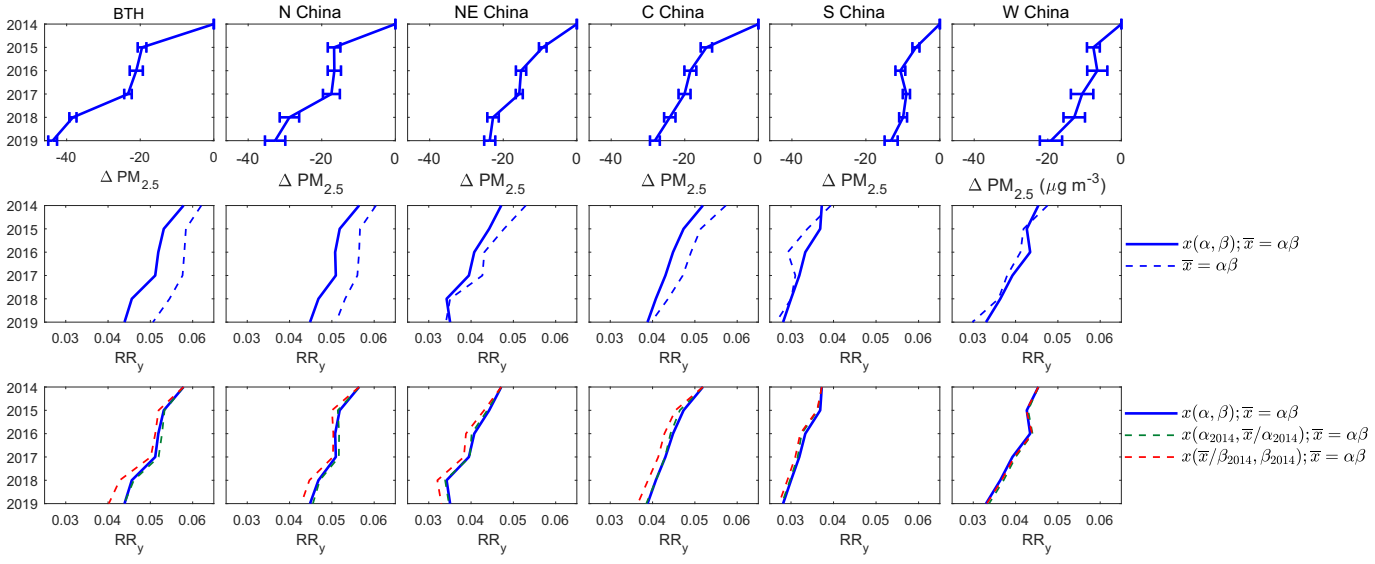

Fig. 10. Annual changes in relative risks (RR_y, unitless) of daily mortality associated with short-term exposure to $PM_{2.5}$ in six Chinese regions between 2014 and 2019. First row: differences in regional annual mean $PM_{2.5}$ concentration relative to 2014 ($\Delta PM_{2.5}$, μg m^{-3}); the error bars indicate the standard deviation in the region for each year. Second row: differences in regional annual relative risks in daily mortality calculated using the observed two-day running-mean $PM_{2.5}$ concentrations (solid line, Section 2.5) and using the annual mean $PM_{2.5}$ concentrations (dashed line). Third row: regional annual relative risks in daily mortality relative to 2014 calculated using the observed $PM_{2.5}$ concentrations (solid line), as well as those calculated using α values for 2014 (green dashed line) and β values for 2014 (red dashed line), respectively. (For interpretation of the references to colour in this figure legend, the reader is referred to the web version of this article.)

6. Conclusions

We combined statistical methods and the GEOS-Chem model to interpret the observed spatiotemporal and probability variations of surface $PM_{2.5}$ concentrations in China from December 2013 to November 2019, with the goal of assessing the drivers for the variations and the implications for public health risks associated with long-term and short-term exposure to $PM_{2.5}$. Annual and seasonal $PM_{2.5}$ concentrations have decreased over most areas in China since 2013, with the largest reductions over the Beijing-Tianjin-Hebei area. The day-to-day variability of $PM_{2.5}$ concentrations over Eastern China showed two distinct major spatial modes that fluctuated in strength seasonally. In winter, similar spatial modes had previously been linked to regional ventilation/accumulation of pollutants associated with winds. However, with the aid of GEOS-Chem simulations, we showed that the dipolar pattern between the BTH and YRD areas, was chemically driven by the secondary formation of sulfate in summer. We stress, however, that the spatial modes identified by the decomposition is sensitive to the distribution of measurement sites, which for our period of study was mostly located in Northern China and coastal provinces as of Eastern and Southern China. The inferred chemical driver, therefore, only applies to these areas well-represented by measurements.

We further used a two-parameter gamma distribution to succinctly represent and interpret the changes in the probability distribution of $PM_{2.5}$. We found that the nationwide decline in seasonal mean $PM_{2.5}$ concentrations mainly reflected decreased occurrences of extremely high $PM_{2.5}$ concentrations, which was in turn strongly driven by the interannual variation of meteorology. These changes in the annual means and PDFs of $PM_{2.5}$ concentrations since December 2013 has led to significant reduction of mortality risks associated with long-term and short-term exposures to $PM_{2.5}$. In particular, regions that were less polluted saw the largest relative benefit per unit decrease in $PM_{2.5}$ concentration due to the steepness of the exposure-response curve at the low-$PM_{2.5}$-concentration end. Better characterization of the exposure-response relationship for different chemical species, for different causes of mortality, and for different parts in China will help us more accurately quantify the health risks associated with $PM_{2.5}$ in the future.

Our integrated statistical analyses and modeling effectively diagnosed the drivers of $PM_{2.5}$ variability and the associated health risks. The identification of the chemical drivers of $PM_{2.5}$ concentration variability can help policy makers to better define emission reduction targets to reduce high $PM_{2.5}$ exposure, as well as to better control species-dependent health risks. In addition, by identifying the connection between the changes in the PDF of $PM_{2.5}$ to the change health risks, we showed health benefits can be gained faster as the emission reduction efforts in the future further reduce the annual mean $PM_{2.5}$ concentrations or the occurrences of very low $PM_{2.5}$ becomes more frequent. As more surface $PM_{2.5}$ measurement sites become available and the model becomes better validated in the future, the model can be further integrated for the assessment of $PM_{2.5}$-health risks on a national scale. We anticipate that our methodology will be used as part of a broader decision tool for the management of $PM_{2.5}$ pollution over China.

Model and data availability

Quality-controlled surface $PM_{2.5}$ concentration data is freely accessible upon request. The GEOS-Chem model (v11-01) is a community model and is freely available (www.geos-chem.org). The model metadata is freely available. The wavelet toolbox package was acquired from (http://paos.colorado.edu/research/wavelets/). EOF decomposition was performed using the functions in NCAR Command Language version 6.4.0 (http://www.ncl.ucar.edu/Applications/eof.shtml).

Author contributions

T.M.F. and P.I.P. designed the study. Z.J. and M.J. performed the analysis and wrote the paper; M.J. ran the GEOS-Chem model calculations. H.T. and Y.M. helped with the processing of raw $PM_{2.5}$ data. All authors contributed to the interpretation of results and the improvement of this paper.

Declaration of competing interest

The authors declare that they have no known competing financial interests or personal relationships that could have appeared to influence the work reported in this paper.

Acknowledgements

This work was supported by the Ministry of Science and Technology, National Key R&D Program of China (2017YFC0209802), by the National Natural Sciences Foundation of China (41975158), and by a Challenge Grant from the Royal Society of London (CHG\R1\170003) from the Royal Society of London. Additional financial support for M.J. and P.I.P. was provided by the UK Natural Environment Research Council (NE/N006879/1).

Appendix A. Supplementary data

Supplementary data to this article can be found online at https://doi.org/10.1016/j.scitotenv.2020.137896.

References

Barrero, M.A., Orza, J.A.G., Cabello, M., Canton, L., 2015. Categorisation of air quality monitoring stations by evaluation of PM10 variability. Sci. Total Environ. 524, 225–236. https://doi.org/10.1016/j.scitotenv.2015.03.138.

Bey, I., Jacob, D.J., Yantosca, R.M., Logan, J.A., Field, B.D., Fiore, A.M., Li, Q., Liu, H.Y., Mickley, L.J., Schultz, M.G., 2001. Global modeling of tropospheric chemistry with assimilated meteorology: model description and evaluation. J. Geophys. Res. 106, 23073–23095. https://doi.org/10.1029/2001JD000807.

Brauer, M., Freedman, G., Frostad, J., Van Donkelaar, A., Martin, R.V., Dentener, F., Van Dingenen, R., Estep, K., Amini, H., Apte, J.S., 2016. Ambient air pollution exposure estimation for the global burden of disease 2013. Environ. Sci. Technol. 50, 79–88. https://doi.org/10.1021/acs.est.5b03709.

Burnett, R.T., Pope, C.A., Ezzati, M., Olives, C., Lim, S.S., Mehta, S., Shin, H.H., Singh, G.M., Hubbell, B.J., Brauer, M., 2014. An integrated risk function for estimating the global burden of disease attributable to ambient fine particulate matter exposure. Environ. Health Perspect. 122, 397–403. https://doi.org/10.1289/ehp.1307049.

Cao, J., Yang, C., Li, J., Chen, R., Chen, B., Gu, D., Kan, H., 2011. Association between long-term exposure to outdoor air pollution and mortality in China: a cohort study. J. Hazard. Mater. 186, 1594–1600. https://doi.org/10.1016/j.jhazmat.2010.12.036.

Cao, J., Xu, H., Xu, Q., Chen, B., Kan, H., 2012. Fine particulate matter constituents and cardiopulmonary mortality in a heavily polluted Chinese City. Environ. Health Perspect. 120, 373–378. https://doi.org/10.1289/ehp.1103671.

Chen, C., Zhu, P., Lan, L., Zhou, L., Liu, R., Sun, Q., Ban, J., Wang, W., Xu, D., Li, T., 2018. Short-term exposures to $PM_{2.5}$ and cause-specific mortality of cardiovascular health in China. Environ. Res. 161, 188–194. https://doi.org/10.1016/j.envres.2017.10.046.

Chen, J., Li, C., Ristovski, Z., Milic, A., Gu, Y., Islam, M.S., Wang, S., Hao, J., Zhang, H.M., He, C., 2017a. A review of biomass burning: emissions and impacts on air quality, health and climate in China. Sci. Total Environ. 579, 1000–1034. https://doi.org/10.1016/j.scitotenv.2016.11.025.

Chen, R., Smith, S.G., Salter, B., El-Gammal, A., Oliveria, J.P., Obminski, C., Watson, R., O'Byrne, P.M., Gauvreau, G.M., Sehmi, R., 2017b. Allergen-induced increases in sputum levels of group 2 innate lymphoid cells in subjects with asthma. Am. J. Respir. Crit. Care Med. 196, 700–712. https://doi.org/10.1164/rccm.201612-2427OC.

Ding, D., Xing, J., Wang, S., Liu, K., Hao, J., 2019. Estimated contributions of emissions controls, meteorological factors, population growth, and changes in baseline mortality to reductions in ambient formula: see text and formula: see text-related mortality in China, 2013-2017. Environ. Health Perspect. 127, 67009. https://doi.org/10.1289/ehp4157.

Fairlie, T.D., Jacob, D.J., Park, R.J., 2007. The impact of transpacific transport of mineral dust in the United States. Atmos. Environ. 41, 1251–1266. https://doi.org/10.1016/j.atmosenv.2006.09.048.

Fang, D., Wang, Q., Li, H., Yu, Y., Lu, Y., Qian, X., 2016. Mortality effects assessment of ambient $PM_{2.5}$ pollution in the 74 leading cities of China. Sci. Total Environ. 569, 1545–1552. https://doi.org/10.1016/j.scitotenv.2016.06.248.

Fountoukis, C., Nenes, A., 2007. ISORROPIA II: a computationally efficient thermodynamic equilibrium model for K+–Ca2+–Mg2+–NH4+–Na+–SO42−–NO 3−–cl−–H2O

aerosols. Atmos. Chem. Phys. 7, 4639–4659. https://doi.org/10.5194/acp-7-4639-2007.
Fu, T.M., Cao, J.J., Zhang, X.Y., Lee, S.C., Zhang, Q., Han, Y.M., Qu, W.J., Han, Z., Zhang, R., Wang, Y.X., Chen, D., Henze, D.K., 2012. Carbonaceous aerosols in China: top-down constraints on primary sources and estimation of secondary contribution. Atmos. Chem. Phys. 12, 2725–2746. https://doi.org/10.5194/acp-12-2725-2012.
Guenther, A.B., Jiang, X., Heald, C.L., Sakulyanontvittaya, T., Duhl, T., Emmons, L.K., Wang, X., 2012. The model of emissions of gases and aerosols from nature version 2.1 (MEGAN2.1): an extended and updated framework for modeling biogenic emissions. Geosci. Model Dev. 5, 1471–1492. https://doi.org/10.5194/gmd-5-1471-2012.
Guo, J., Miao, Y., Zhang, Y., Liu, H., Li, Z., Zhang, W., He, J., Lou, M., Yan, Y., Bian, L., Zhai, P., 2016. The climatology of planetary boundary layer height in China derived from radiosonde and reanalysis data. Atmos. Chem. Phys. 16, 13309–13319. https://doi.org/10.5194/acp-16-13309-2016.
He, J., Gong, S., Yu, Y., Yu, L., Wu, L., Mao, H., Song, C., Zhao, S., Liu, H., Li, X., Li, R., 2017. Air pollution characteristics and their relation to meteorological conditions during 2014-2015 in major Chinese cities. Environ. Pollut. 223, 484–496. https://doi.org/10.1016/j.envpol.2017.01.050.
Hou, X., Zhu, B., Kumar, K.R., Lu, W., 2019. Inter-annual variability in fine particulate matter pollution over China during 2013–2018: role of meteorology. Atmos. Environ. 214, 116842. https://doi.org/10.1016/j.atmosenv.2019.116842.
Huang, X., Liu, Z., Liu, J., Hu, B., Wen, T., Tang, G., Zhang, J., Wu, F., Ji, D., Wang, L., Wang, Y., 2017. Chemical characterization and source identification of $PM_{2.5}$ at multiple sites in the Beijing–Tianjin–Hebei region, China. Atmos. Chem. Phys. 17, 12941–12962. https://doi.org/10.5194/acp-17-12941-2017.
Husak, G., Michaelsen, J., Funk, C.C., 2007. Use of the gamma distribution to represent monthly rainfall in Africa for drought monitoring applications. Int. J. Climatol. 27, 935–944. https://doi.org/10.1002/joc.1441.
Jaeglé, L., Quinn, P.K., Bates, T.S., Alexander, B., Lin, J.-T., 2011. Global distribution of sea salt aerosols: new constraints from in situ and remote sensing observations. Atmos. Chem. Phys. 11, 3137–3157. https://doi.org/10.5194/acp-11-3137-2011.
Lee, H., Honda, Y., Hashizume, M., Guo, Y.L., Wu, C.-F., Kan, H., Jung, K., Lim, Y.-H., Yi, S., Kim, H., 2015. Short-term exposure to fine and coarse particles and mortality: a multicity time-series study in East Asia. Environ. Pollut. 207, 43–51. https://doi.org/10.1016/j.envpol.2015.08.036.
Leung, D.M., Tai, A.P.K., Mickley, L.J., Moch, J.M., van Donkelaar, A., Shen, L., Martin, R.V., 2018. Synoptic meteorological modes of variability for fine particulate matter ($PM_{2.5}$) air quality in major metropolitan regions of China. Atmos. Chem. Phys. 18, 6733–6748. https://doi.org/10.5194/acp-18-6733-2018.
Li, H., Chen, R., Meng, X., Zhao, Z., Cai, J., Wang, C., Yang, C., Kan, H., 2015. Short-term exposure to ambient air pollution and coronary heart disease mortality in 8 Chinese cities. Int. J. Cardiol. 197, 265–270. https://doi.org/10.1016/j.ijcard.2015.06.050.
Li, M., Zhang, Q., Streets, D.G., He, K.B., Cheng, Y.F., Emmons, L.K., Huo, H., Kang, S.C., Lu, Z., Shao, M., Su, H., Yu, X., Zhang, Y., 2014. Mapping Asian anthropogenic emissions of non-methane volatile organic compounds to multiple chemical mechanisms. Atmos. Chem. Phys. 14, 5617–5638. https://doi.org/10.5194/acp-14-5617 2014.
Li, M., Zhang, Q., Kurokawa, J.-i., Woo, J.-H., He, K., Lu, Z., Ohara, T., Song, Y., Streets, D.G., Carmichael, G.R., Cheng, Y., Hong, C., Huo, H., Jiang, X., Kang, S., Liu, F., Su, H., Zheng, B., 2017. MIX: a mosaic Asian anthropogenic emission inventory under the international collaboration framework of the MICS-Asia and HTAP. Atmos. Chem. Phys. 17, 935–963. https://doi.org/10.5194/acp-17-935-2017.
Lin, J., Mcelroy, M.B., 2010. Impacts of boundary layer mixing on pollutant vertical profiles in the lower troposphere: implications to satellite remote sensing. Atmos. Environ. 44, 1726–1739. https://doi.org/10.1016/j.atmosenv.2010.02.009.
Liu, C., Chen, R., Sera, F., Vicedocabrera, A.M., Guo, Y., Tong, S., Coelho, M.D.S.Z.S., Saldiva, P., Lavigne, E., Matus, P., 2019. Ambient particulate air pollution and daily mortality in 652 cities. N. Engl. J. Med. 381, 705–715. https://doi.org/10.1056/NEJMoa1817364.
Liu, M., Lin, J., Wang, Y., Sun, Y., Zheng, B., Shao, J., Chen, L., Zheng, Y., Chen, J., Fu, M., 2018. Spatiotemporal variability of NO_2 and $PM_{2.5}$ over eastern China: observational and model analyses with a novel statistical method. Atmos. Chem. Phys. 18, 12933–12952. https://doi.org/10.5194/acp-18-12933-2018.
Lorenz, E.N., 1956. Empirical orthogonal functions and statistical weather prediction. Sci. Rep. 409, 997–999. https://doi.org/10.1134/S1028334X06060377.
Ma, Q., Cai, S., Wang, S., Zhao, B., Martin, R.V., Brauer, M., Cohen, A., Jiang, J., Zhou, W., Hao, J., Frostad, J., Forouzanfar, M.H., Burnett, R.T., 2017. Impacts of coal burning on ambient $PM_{2.5}$ pollution in China. Atmos. Chem. Phys. 17, 4477–4491. https://doi.org/10.5194/acp-17-4477-2017.
Mao, J., Paulot, F., Jacob, D.J., Cohen, R.C., Crounse, J.D., Wennberg, P.O., Keller, C.A., Hudman, R.C., Barkley, M.P., Horowitz, L.W., 2013. Ozone and organic nitrates over the eastern United States: sensitivity to isoprene chemistry. J. Geophys. Res. 118. https://doi.org/10.1002/jgrd.50817.
Mao, L., Liu, R., Liao, W., Wang, X., Shao, M., Liu, S.C., Zhang, Y., 2019. An observation-based perspective of winter haze days in four major polluted regions of China. Natl. Sci. Rev. 6, 515–523. https://doi.org/10.1093/nsr/nwy118.
Marani, A., Lavagnini, I., Buttazzoni, C., 1986. Statistical study of air pollutant concentrations via generalized gamma distributions. J. Air Pollut. Control. Assoc. 36, 1250–1254. https://doi.org/10.1080/00022470.1986.10466173.
Ministry of Ecology and Environment of the People's Republic of China, 2018. Report on the State of the Ecology and Environment of China, 2017. http://english.mee.gov.cn/Resources/Reports/soe/SOEE2017/201808/P020180801597738742758.pdf.
Ministry of Environmental Protection of the People's Republic of China, 2012. Ambient Air Quality Standards (GB3095–2012).
Ministry of Environmental Protection of the People's Republic of China, 2013a. Specifications and Test Procedures for Ambient Air Quality Continuous Automated Monitoring System for PM_{10} and $PM_{2.5}$. (HJ653–2013).
Ministry of Environmental Protection of the People's Republic of China, 2013b. Technical regulation for selection of ambient air quality monitoring stations (on trial) (HJ664-2013).
Ministry of Environmental Protection of the People's Republic of China, 2015. Report on the State of the Environment of China, 2014. http://english.mee.gov.cn/Resources/Reports/soe/soe2011/201606/P020160601592064474593.pdf.
Ministry of Environmental Protection of the People's Republic of China, 2016. Report on the State of the Environment of China, 2015. http://english.mee.gov.cn/Resources/Reports/soe/Report/201706/P020170614504782926467.pdf.
Ministry of Environmental Protection of the People's Republic of China, 2017. Report on the State of the Environment of China, 2016. http://english.mee.gov.cn/Resources/Reports/soe/ReportSOE/201709/P020170929573904364594 .pdf.
Parrella, J.P., Jacob, D.J., Liang, Q., Zhang, Y., Mickley, L.J., Miller, B.F., Evans, M.J., Yang, X., Pyle, J.A., Theys, N., 2012. Tropospheric bromine chemistry: implications for present and pre-industrial ozone and mercury. Atmos. Chem. Phys. 12, 6723–6740. https://doi.org/10.5194/acp-12-6723-2012.
Philip, S., Martin, R., Snider, G., Weagle, C., Donkelaar, A., Brauer, M., Henze, D., Klimont, Z., Venkataraman, C., Guttikunda, S., 2017. Anthropogenic fugitive, combustion and industrial dust is a significant, underrepresented fine particulate matter source in global atmospheric models. Environ. Res. Lett. 12. https://doi.org/10.1088/1748-9326/aa65a4.
Pye, H.O.T., Seinfeld, J.H., 2010. A global perspective on aerosol from low-volatility organic compounds. Atmos. Chem. Phys. 10, 4377–4401. https://doi.org/10.5194/acp-10-4377-2010.
Pye, H.O.T., Liao, H., Wu, S., Mickley, L.J., Jacob, D.J., Henze, D.K., Seinfeld, J.H., 2009. Effect of changes in climate and emissions on future sulfate-nitrate-ammonium aerosol levels in the United States. J. Geophys. Res. 114. https://doi.org/10.1029/2008JD010701.
Pope, C.A., Burnett, R.T., Thun, M.J., Calle, E.E., Krewski, D., Ito, K., Thurston, G.D., 2002. Lung cancer, cardiopulmonary mortality, and long-term exposure to fine particulate air pollution. JAMA (Journal of the American Medical Association) 287, 1132–1141. https://doi.org/10.1001/jama.287.9.1132.
Pye, H.O.T., Chan, A.W.H., Barkley, M.P., Seinfeld, J.H., 2010. Global modeling of organic aerosol: the importance of reactive nitrogen. Atmos. Chem. Phys. 10, 21259–21301. https://doi.org/10.5194/acpd-10-21259-2010.
Quan, J., Tie, X., Qiang, Z., Quan, L., Xia, L., Yang, G., Zhao, D., 2014. Characteristics of heavy aerosol pollution during the 2012–2013 winter in Beijing, China. Atmos. Environ. 88, 83–89. https://doi.org/10.1016/j.atmosenv.2014.01.058.
Robinson, A.L., Donahue, N.M., Shrivastava, M., Weitkamp, E.A., Sage, A.M., Grieshop, A.P., Lane, T.E., Pierce, J.R., Pandis, S.N., 2007. Rethinking Organic Aerosols: Semivolatile Emissions and Photochemical Aging. Science 315, 1259–1262. https://doi.org/10.1126/science.1133061.
Rumberg, B., Alldredge, R., Claiborn, C., 2001. Statistical distributions of particulate matter and the error associated with sampling frequency. Atmos. Environ. 35 (16), 2907–2920. https://doi.org/10.1016/s1352-2310(00)00554-9.
Shang, Y., Sun, Z., Cao, J., Wang, X., Zhong, L., Bi, X., Li, H., Liu, W., Zhu, T., Huang, W., 2013. Systematic review of Chinese studies of short-term exposure to air pollution and daily mortality. Environ. Int. 54, 100–111. https://doi.org/10.1016/j.envint.2013.01.010.
Sharma, P., Sharma, P., Jain, S., Kumar, P., 2013. An integrated statistical approach for evaluating the exceedence of criteria pollutants in the ambient air of megacity Delhi. Atmos. Environ. 70, 7–17. https://doi.org/10.1016/j.atmosenv.2013.01.004.
Shi, Y., Matsunaga, T., Yamaguchi, Y., Zhao, A., Li, Z., Gu, X., 2018. Long-term trends and spatial patterns of PM2.5-induced premature mortality in south and Southeast Asia from 1999 to 2014. Sci. Total Environ., 1504–1514 https://doi.org/10.1016/j.scitotenv.2018.03.146.
Shu, L., Xie, M., Gao, D., Wang, T., Fang, D., Liu, Q., Huang, A., Peng, L., 2017. Regional severe particle pollution and its association with synoptic weather patterns in the Yangtze River Delta region, China. Atmos. Chem. Phys. 17, 12871–12891. https://doi.org/10.5194/acp-17-12871-2017.
Silver, B., Reddington, C.L., Arnold, S.R., Spracklen, D.V., 2018. Substantial changes in air pollution across China during 2015–2017. Environ. Res. Lett. 13, 114012. https://doi.org/10.1088/1748-9326/aae718.
Son, J., Lee, J., Kim, K., Jung, K., Bell, M.L., 2012. Characterization of fine particulate matter and associations between particulate chemical constituents and mortality in Seoul, Korea. Environ. Health Perspect. 120, 872–878. https://doi.org/10.1289/ehp.1104316.
Song, C., He, J., Wu, L., Jin, T., Chen, X., Li, R., Ren, P., Zhang, L., Mao, H., 2017. Health burden attributable to ambient $PM_{2.5}$ in China. Environ. Pollut. 223, 575–586. https://doi.org/10.1016/j.envpol.2017.01.060.
Stacy, E.W., 1962. A generalization of the gamma distribution. Ann. Math. Stat. 33, 1187–1192. https://doi.org/10.1214/aoms/1177704481.
Sui, Y., Jiang, D., Tian, Z., 2013. Latest update of the climatology and changes in the seasonal distribution of precipitation over China. Theor. Appl. Climatol. 113, 599–610. https://doi.org/10.1007/s00704-012-0810-z.
The State Council of the People's Republic of China, 2013. Air Pollution Prevention and Control Action Plan. http://www.gov.cn/zhengce/content/2013-09/13/content_4561.htm (Last accessed: 9th March, 2020).
Torrence, C., Compo, G.P., 1998. A practical guide to wavelet analysis. Bull. Am. Meteorol. Soc. 79, 61–78. https://doi.org/10.1175/1520-0477(1998)079<0061:APGTWA>2.0.CO;2.
Turap, Y., Talifu, D., Wang, X., Abulizi, A., Maihemuti, M., Tursun, Y., Ding, X., Aierken, T., Rekefu, S., 2019. Temporal distribution and source apportionment of PM2.5 chemical composition in Xinjiang, NW-China. Atmos. Res. 218, 257–268. https://doi.org/10.1016/j.atmosres.2018.12.010.

Turpin, B.J., Lim, H., 2001. Species contributions to $PM_{2.5}$ mass concentrations: revisiting common assumptions for estimating organic mass. Aerosol Sci. Technol. 35, 602–610. https://doi.org/10.1080/02786820152051454.

van der Werf, G.R., Randerson, J.T., Giglio, L., Collatz, G.J., Mu, M., Kasibhatla, P.S., Morton, D.C., DeFries, R.S., Jin, Y., van Leeuwen, T.T., 2010. Global fire emissions and the contribution of deforestation, savanna, forest, agricultural, and peat fires (1997–2009). Atmos. Chem. Phys. 10, 11707–11735. https://doi.org/10.5194/acp-10-11707-2010.

World Health Organization. Occupational and Environmental Health Team, 2006. WHO Air Quality Guidelines for Particulate Matter, Ozone, Nitrogen Dioxide and Sulfur Dioxide: Global Update 2005: Summary of Risk Assessment. World Health Organization, Geneva http://www.who.int/iris/handle/10665/69477.

Xue, J., Li, J., Zhang, X., 2010. Characteristics of elemental compositions of ambient PM2.5 during sandstorm in spring in Xinjiang. J. Environ. Health 27, 759–762.

Yang, Y., Wang, H., Smith, S.J., Ma, P.-L., Rasch, P.J., 2017. Source attribution of black carbon and its direct radiative forcing in China. Atmos. Chem. Phys. 17, 4319–4336. https://doi.org/10.5194/acp-17-4319-2017.

Zender, C.S., Bian, H., Newman, D., 2003. Mineral dust entrainment and deposition (DEAD) model: description and 1990s dust climatology. J. Geophys. Res. Atmos. 108. https://doi.org/10.1029/2002JD002775.

Zhai, S., Jacob, D.J., Wang, X., Shen, L., Li, K., Zhang, Y., Gui, K., Zhao, T., Liao, H., 2019. Fine particulate matter ($PM_{2.5}$) trends in China, 2013–2018: separating contributions from anthropogenic emissions and meteorology. Atmos. Chem. Phys. 19, 11031–11041. https://doi.org/10.5194/acp-19-11031-2019.

Zhang, L., Shao, J., Lu, X., Zhao, Y., Hu, Y., Henze, D.K., Liao, H., Gong, S., Zhang, Q., 2016. Sources and processes affecting fine particulate matter pollution over North China: an Adjoint analysis of the Beijing APEC period. Environ. Sci. Technol. 50, 8731–8740. https://doi.org/10.1021/acs.est.6b03010.

Zhang, Q., Zheng, Y., Tong, D., Shao, M., Wang, S., Zhang, Y., Xu, X., Wang, J., He, H., Liu, W., 2019. Drivers of improved PM2.5 air quality in China from 2013 to 2017. PNAS 116, 24463–24469. https://doi.org/10.1073/pnas.1907956116.

Zhang, X., Wang, Y., Niu, T., Zhang, X., Gong, S.L., Zhang, Y., Sun, J.Y., 2011. Atmospheric aerosol compositions in China: spatial/temporal variability, chemical signature, regional haze distribution and comparisons with global aerosols. Atmos. Chem. Phys. 12, 779–799. https://doi.org/10.5194/acp-12-779-2012.

Zhang, Y., Cai, J., Wang, S., He, K., Zheng, M., 2017. Review of receptor-based source apportionment research of fine particulate matter and its challenges in China. Sci. Total Environ. 586, 917–929. https://doi.org/10.1016/j.scitotenv.2017.02.071.

Zhang, Y.L., Cao, F., 2015. Fine particulate matter ($PM_{2.5}$) in China at a city level. Sci. Rep. 5, 14884. https://doi.org/10.1038/srep14884.

Zhao, X., Zhang, X., Xu, X., Xu, J., Meng, W., Pu, W., 2009. Seasonal and diurnal variations of ambient $PM_{2.5}$ concentration in urban and rural environments in Beijing. Atmos. Environ. 43, 2893–2900. https://doi.org/10.1016/j.atmosenv.2009.03.009.

Zheng, B., Tong, D., Li, M., Liu, F., Hong, C., Geng, G., Li, H., Li, X., Peng, L., Qi, J., Yan, L., Zhang, Y., Zhao, H., Zheng, Y., He, K., Zhang, Q., 2018. Trends in China's anthropogenic emissions since 2010 as the consequence of clean air actions. Atmos. Chem. Phys. 18, 14095–14111. https://doi.org/10.5194/acp-18-14095-2018.

Zhong, J., Zhang, X., Dong, Y., Wang, Y., Liu, C., Wang, J., Zhang, Y., Che, H., 2018. Feedback effects of boundary-layer meteorological factors on cumulative explosive growth of $PM_{2.5}$ during winter heavy pollution episodes in Beijing from 2013 to 2016. Atmos. Chem. Phys. 18, 247–258. https://doi.org/10.5194/acp-18-247-2018.

Zhou, M., Wang, H., Zhu, J., Chen, W., Wang, L., Liu, S., Li, Y., Wang, L., Liu, Y., Yin, P., 2016. Cause-specific mortality for 240 causes in China during 1990–2013: a systematic subnational analysis for the Global Burden of Disease Study 2013. Lancet 387, 251–272. https://doi.org/10.1016/S0140-6736(15)00551-6.

Ministry of Ecology and Environment of the People's Republic of China, 2019. Report on the State of the Ecology and Environment of China, 2018, http://www.mee.gov.cn/hjzl/sthjzk/zghjzkgb/201905/P020190619587632630618.pdf.

Ministry of Environmental Protection of the People's Republic of China, 2014. Report on the State of the Environment of China, 2013, http://english.mee.gov.cn/Resources/Reports/soe/soe2011/201606/P020160601591756378883.pdf.